J|A|C|S
ARTICLES
Published on Web 12/17/2005

Dynamics of Electron Transport by Elastic Bending of Short DNA Duplexes. Experimental Study and Quantitative Modeling of the Cyclic Voltammetric Behavior of 3′-Ferrocenyl DNA End-Grafted on Gold

Agnès Anne* and Christophe Demaille*

Contribution from the Laboratoire d'Electrochimie Moléculaire, Unité Mixte de Recherche Université - CNRS No. 7591, Université de Paris 7 - Denis Diderot, 2 place Jussieu, 75251 Paris Cedex 05, France

Received July 28, 2005; E-mail: demaille@paris7.jussieu.fr

Abstract: The dynamics of electron transport within a molecular monolayer of 3′-ferrocenylated-$(dT)_{20}$ strands, 5′-thiol end-grafted onto gold electrode surfaces via a short C2-alkyl linker, is analyzed using cyclic voltammetry as the excitation/measurement technique. It is shown that the single-stranded DNA layer behaves as a diffusionless system, due to the high flexibility of the ss-DNA chain. Upon hybridization by the fully complementary $(dA)_{20}$ target, the DNA-modified gold electrode displays a highly unusual voltammetric behavior, the faradaic signal even ultimately switching off at a high enough potential scan rate. This remarkable extinction phenomenon is qualitatively and quantitatively justified by the model of elastic bending diffusion developed in the present work which describes the motion of the DNA-borne ferrocene moiety as resulting from the elastic bending of the duplex DNA toward and away from the electrode surface. Its use allows us to demonstrate that the dynamics of electron transport within the hybridized DNA layer is solely controlled by the intrinsic bending elasticity of ds-DNA. Fast scan rate cyclic voltammetry of end-grafted, redox-labeled DNA layers is shown to be an extremely efficient method to probe the bending dynamics of short-DNA fragments in the submillisecond time range. The persistence length of the end-anchored ds-DNA, a parameter quantifying the flexibility of the nanometer-long duplex, can then be straightforwardly and accurately determined from the voltammetry data.

Introduction

The notion of deformability of biological macromolecules in general, and of nucleic acids in particular, is well-understood and widely used by physicists and biologists for studying and modeling molecular recognition processes.[1] This concept is also increasingly exploited in the modern field of electrochemical DNA hybridization sensors or biochips. For these recent applications, the static conformational changes of a DNA oligonucleotide monolayer end-tethered to an electrode surface, which occur upon hybridization with a complementary single-stranded (ss) DNA sequence in solution, are exploited to modulate the electrochemical response of the sensor which, depending on the experimental design and the type of grafted DNA, can be either "switched on"[2] or "switched off."[3] Most of these well-defined systems involve the use of a redox label borne by the free terminus of grafted DNA, whose distance from the electrode surface is altered as a result of the conformational changes accompanying the hybridization of the grafted strand: repositioning of the redox probe closer or further away from the electrode surface respectively turning the sensor "on" or "off".

Scheme 1

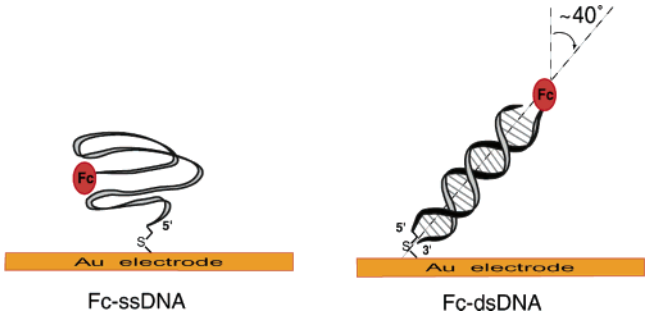

In this framework, we recently presented and characterized, by fast cyclic voltammetry, a switch-off type system consisting of a molecular monolayer of 20-mer ssDNA chains ($(dT)_{20}$ oligonucleotide) anchored by their 5′-thiol end onto a gold electrode surface via a short C2-alkyl linker and 3′-end-labeled by a redox-active ferrocene moiety (Scheme 1).[4]

Within this remarkably stable, low density "model" system, the molecular recognition capability of the DNA chains was

(1) Samori, B.; Zuccheri, G. *Angew. Chem., Int. Ed.* **2005**, *44*, 1166−1181.
(2) (a) Gooding, J. J.; Chou, A.; Mearns, F. Y.; Wong, E.; Jericho, K. L. *Chem. Commun.* **2003**, 1938−1939. (b) Immoos, C. E.; Lee, S. J.; Grinstaff, M. W. *J. Am. Chem. Soc.* **2004**, *126*, 10814−10815.
(3) (a) Fan, C; Plaxco, K. W.; Hegger, A. J. *Proc. Natl. Acad. Sci. U.S.A.* **2003**, *100*, 9134−9137. (b) Immoos, C. E.; Lee, S. J.; Grinstaff, M. W. *ChemBioChem* **2004**, *5*, 1100−1103. (c) Paleèek, E. *Trends Biotechnol.* **2004**, *22*, 55−58.
(4) Anne, A.; Bouchardon, A.; Moiroux, J. *J. Am. Chem. Soc.* **2003**, *125*, 1112−1113.

10.1021/ja055112a CCC: $33.50

kept intact, allowing us to evidence *qualitatively* that, beyond the simple notion of hybridization-induced repositioning of the redox probe, analysis of the electrochemical response of the redox-labeled DNA layer could give access to the *time dependent motion* of the DNA chain, i.e., to its *dynamics*.

Probing the dynamics of a DNA fragment is, in itself, of great interest as this is one of the rare approaches allowing the mechanical properties of *nanometer-long* double-stranded (ds) DNA to be determined.[5a] Moreover, DNA dynamics is usually experimentally observed using sophisticated spectroscopic techniques and has never been addressed electrochemically.[5b]

Electrochemical characterization of molecular layers of end-grafted redox-labeled dsDNA has, on the opposite, been intensively used to examine the electron transport properties of dsDNA,[6−8] but most of these works neglected DNA chain motion as a possible charge transport mechanism. However, the relevance of DNA flexibility to electron transport along duplex DNA is now increasingly recognized since recent theoretical calculations,[9] and real-time spectroscopic results,[10] tend to show that electron propagation, over distances longer than a few base pairs, necessarily requires coupling of base-to-base electron hopping with conformational rearrangement of the bases, induced by the elastic deformation of the strand.[10d] The intertwinement of these two components of electron transport makes extremely difficult the full quantitative modeling of electron propagation along duplex DNA. In the experimental system we have developed, consisting of a molecular layer of end-grafted redox DNA, the electron transfer is thermodynamically perfectly well-defined as it occurs between the electrode surface and the ferrocenyl head (Fc), borne by the free 5′ terminus of the duplex DNA (Scheme 1). Moreover, considering the low redox potential of the chosen alkyl-ferrocene moiety (∼150 mV/SCE), the generation of a hole in the DNA base stack, and ensuing electron hopping between neighboring bases, is totally excluded. Electron transport within our system thus solely relies on the movement of the DNA-borne ferrocene head toward and away from the electrode surface. Analysis of the electrochemical response of the system therefore allows us to assess the role of the elastic deformation of the duplex on electron transport by DNA.

The aim of the present work is to conduct a detailed analysis of the electrochemical response of the system using fast cycling voltammetry, a time-resolved technique reflecting the motion of the DNA-borne ferrocene probe, to access, and *quantitatively model*, the dynamics of electron transport by the *elastic motion* of short, end-grafted, double-stranded DNA. We show below that the highly unusual voltammetric behavior of the hybridized Fc-DNA layer reflects the elastic *bending motion* of the quite rigid DNA duplex, bringing the ferrocene head in contact with the electrode surface. Appropriate modeling of such an elastic bending diffusion then allows us to fully account for the observed voltammetric behavior throughout the range of potential scan rates (i.e., observation times) explored: from low scan rates, at which the dsDNA rod is given enough time to bring its Fc head in contact with the electrode surface, up to the highest scan rates, at which dsDNA appears as frozen in time. Analysis of the voltammetric data, in light of our elastic bending diffusion model, yields the persistence length of the end-anchored double-stranded DNA, a parameter quantifying the elasticity of the duplex, and allows us to demonstrate that the flexible bending motion of the DNA double helix can be, in itself, a very efficient charge transport mechanism. Fast scan rate cyclic voltammetry of end-grafted, redox-labeled DNA layers is shown to be a powerful method to probe the bending dynamics of short DNA fragments in the sub-millisecond time range.

Scheme 2. Synthesis of 5′-Cystaminyl 3′-Ferrocene-Labeled-$(dT)_{20}$ Oligonucleotide **3** and Its Subsequent Reduction to Its 5′-Thiol Deprotected Form **4**[a]

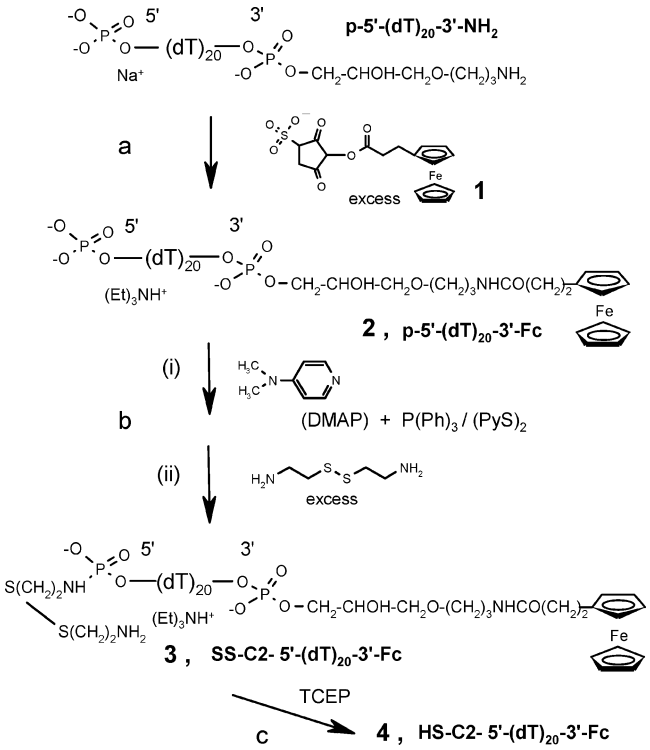

[a] (a) Fc-NHS, aq. phosphate, pH 8, rt, 3 h, 90%; (b) (i) DMAP: dimethylamino-pyridine, $P(Ph)_3/(PyS)_2$, DMSO, rt, 15 min, (ii) cystamine, 3 h, 30%; (c) TCEP: [tris(2-carboxyethyl)phosphine], Tris buffer, rt, 16 h, >90% (HPLC analysis).

Experimental Section

Materials. All DNA oligonucleotides were purchased from Apibio (Grenoble, France) as their sodium salts at a 0.2−1 μmol scale and were HPLC purified grade products. The modified oligonucleotide p-5′-$(dT)_{20}$-3′-NH_2 used as the precursor sequence for chemical synthesis of 5′-C2-thiolated-3′-ferrocenylated oligonucleotide **4** (see Scheme 2) carries a 3′-TFA (C7) Aminolinker = $-(CH_2)CHOHCH_2O-(CH_2)_3-NH_2$.

All chemicals and solvents were analytical grade and used without further purification.

(5) (a) Lankaš, F. *Biopolymers* **2004**, *73*, 327−339 and references therein. (b) Okonogi, T. M.; Reese, A. W.; Alley, S. C.; Hopkins, P. B.; Robinson, B. H. *Biophys. J.* **1999**, *77*, 3256−3276.
(6) Hartwich, G.; Caruana, D. J.; de Lumley-Woodyear, T.; Wu, Y.; Campbell, C. N.; Heller, A. *J. Am. Chem. Soc.* **1999**, *121*, 10803−10812.
(7) Kelley, S. O.; Jackson, N. M.; Hill, M. G.; Barton, J. K. *Angew. Chem., Int. Ed.* **1999**, *38*, 941−945.
(8) Long, Y.-T.; Li, C.-Z.; Sutherland, T. C.; Chahma, M.; Lee, J. S.; Kraatz, H.-B. *J. Am. Chem. Soc.* **2003**, *125*, 8724−8725.
(9) (a) Berlin, Y. A.; Burin, A. L.; Siebbeles, L. D. A.; Ratner, M. A. *J. Phys. Chem. A* **2001**, *105*, 5666−5678. (b) Renger, T.; Marcus, R. A. *J. Phys. Chem. A* **2003**, *107*, 8404−8419. (c) Matulewski, J.; Baranovskii, S. D.; Thomas, P. *Phys. Chem. Chem. Phys.* **2005**, *7*, 1514−1517.
(10) (a) O'Neill, M. A.; Becker, H.-C.; Wan, C.; Barton, J. K.; Zewail, A. H. *Angew. Chem., Int. Ed.* **2003**, *42*, 5896−5900. (b) O'Neill, M. A.; Barton, J. K. *J. Am. Chem. Soc.* **2004**, *126*, 11471−11483. (c) O'Neill, M. A.; Barton, J. K. *J. Am. Chem. Soc.* **2004**, *126*, 13234−13235. (d) Kaden, P.; Mayer-Enthart, E.; Trifonov, A.; Fiedig, T.; Wagenknecht, H.-A. *Angew. Chem., Int. Ed.* **2005**, *44*, 1636−1639.

All reactions were carried out in polypropylene tubes under an inert atmosphere at ambient temperature (20−25 °C) and protected from light. All aqueous solutions were made with Milli-Q purified water (Millipore). Phosphate buffers were made of 49 mM or 74 mM KH_2PO_4, pH adjusted to 7.0 or 8.0, respectively, with a 1 M NaOH solution.

Chromatography. Reversed-phase high-performance liquid chromatography (HPLC) was performed with a Gilson 305/306 HPLC pump system equipped with a Gilson 119 UV−vis detector operating at 270 nm, using a Macherey−Nagel Nucleosil 120-5 C18 (4.6 mm ID × 15 cm) analytical column. Pump control and data processing used a Gilson Unipoint LC software (for Windows). Unless otherwise specified, the eluent conditions were as follows: solvent A, 10% acetonitrile in aqueous triethylammonium acetate, Et_3NH^+, AcO^- (TEAA, 0.1 M) pH adjusted to 7.0 with acetic acid; solvent B, acetonitrile. Elutions were done with a linear gradient from 5% to 25% B in 20 min. The flow rate was 0.8 mL/min.

Spectrometries. UV−visible spectra and optical density (OD) were measured on a Hewlett-Packard HP 8452 diode array spectrophotometer. The concentration of oligonucleotides were estimated by UV absorption at 260 nm, assuming a molar absorptivity coefficient ϵ_{260} of 15 400, 6700, for dA and dT,[11] and taking an average ϵ_{260} of 9500 M^{-1} cm^{-1} for the ferrocene moiety. DNA melting curves were obtained by monitoring the absorbance of DNA solutions at 260 nm as a function of temperature. The melting temperatures T_m were measured in 0.1 M $NaClO_4$, 25 mM sodium phosphate (pH 7.0) solutions containing 2 μM oligonucleotide each, T_m data being estimated to be accurate within 1 °C.

Matrix-assisted laser desorption/ionization time-of-flight (MALDI-TOF) mass spectra were obtained from the Université Pierre et Marie Curie, Laboratoire de Chimie Structurale Organique et Biologique (Paris, France) on a PerSeptive Biosystems Inc. (Framingham, MA) Voyager Elite instrument operating in the positive mode using 2,4,6-trihydroxyacetophenone in diammonium citrate as the matrix and 274 nm pulsed light. Internal calibration was carried out using the nucleotide sequence $d(A_{11}T_7G_5C_5)$ (M 8604.6) in the above matrix.

Cyclic Voltammetry Measurements. Aqueous 1 M $NaClO_4$ containing 25 mM phosphate buffer (pH 7.0) was used as the electrolyte solution for all electrochemical studies. Electrochemical experiments were performed with a conventional three-electrode configuration consisting of a gold-disk working electrode, a platinum wire counter electrode, and a reference electrode, being a Ag/AgCl wire (calibrated with 1mM ferrocenemethanol) for studies at bare-gold electrodes, or a KCl saturated calomel electrode (*SCE*) for studies of DNA-modified-gold electrodes. The *SCE* reference electrode was separated from the supporting electrolyte solution with a bridge terminated with a glass frit, containing an aqueous solution of 1 M NaCl. The peak potentials were measured with an accuracy of ±5 mV. Solution-phase studies at bare electrodes were carried out in a one-compartment microcell with a working volume of ca. 100 μL.

For potential scan rates ν up to 200 V/s, all electrochemical experiments were performed using a conventional instrumentation equipment.[12a] For high scan rate cyclic voltammetry of the DNA-modified electrodes, the signal generator was a Hewlett-Packard 3314A, and the curves were recorded with a Tektronix TDS 430A oscilloscope with a minimum acquisition time of 5 ns per point; a home-built potentiostat with a large bandwidth was used.[13] This ultrafast equipment, associated with a low solution ohmic drop, rendered minimal by the high conductivity of aqueous 1 M $NaClO_4$ supporting electrolyte, allowed the reliable electrochemical measurement of grafted Fc-DNA electrode responses with no detectable distortion of the signals.

Cyclic voltammograms were recorded without ohmic drop compensation. All potentials are reported versus *SCE*. The temperature in all electrochemical experiments was 21 °C.

Pretreatment of the Polycrystalline Gold Electrodes. Gold disk working electrodes were constructed by sealing lengths of gold wire (99.99%, Goodfellow) (0.5 mm or 125 μm diameter) within polypropylene bodies or (12.5 μm diameter) in soft glass. For all experiments, the electrodes were polished to a mirror finish using progressively finer grades of alumina polishing suspensions (3, 0.5, and 0.05 μm, Buehler) followed by ultrasonication in water and ethanol. *For preparation of Fc-$(dT)_{20}$ monolayers*, the freshly polished electrodes were electrochemically cleaned by cyclic voltammetry at the scan rate 0.2 V s^{-1} in 1 N H_2SO_4 as reported previously.[14] The final electrochemical oxidation step was followed by electrochemical reduction of the gold oxide monolayer via a reverse potential scan down to +0.2 V. The thus pretreated gold electrodes were quickly rinsed with water and ethanol and then immediately used for reaction with thiol-deprotected **4**. The effective areas of the electrodes S_{eff} were derived from the charge associated with the gold oxide reduction peak and typically correspond to a roughness factor of ca. 3.

Preparation of the Fc-$(dT)_{20}$-Modified Gold Electrodes. The 5′-thiolated-oligonucleotide **3** was kept until use under its oxidized $-(CH_2)_2-S-S-(CH_2)_2-NH_2$ form in order to protect the thiol group from undesired oxidation or disulfide dimers. In a typical procedure, reduction of an appropriate amount of 5′-cystaminyl 20-mer oligonucleotide **4** (∼0.45 OD_{260} units, 5 nmol) was effected by treatment with tris(2-carboxyethyl)phosphine (TCEP, HCl) (28 nmol) in 5 μL of 0.1 M Tris·HCl (pH 7.5) under an inert atmosphere. The reaction was allowed to proceed overnight at room temperature to allow complete reduction of the disulfide bond as judged by RP-HPLC analysis (for a typical HPLC profile of the deprotection reaction, see Supporting Information, Figure 1b supplied in ref 4). The resulting reduction product HS−C2−5′-$(dT)_{20}$-3′-Fc **4** was purified from excess reagent by RP-HPLC and collected in a polypropylene tube. After acetonitrile removal by passing an inert gas, the thiol sample was used for direct thiolation of gold electrode surfaces as follows. 50 μL (∼20−50 μM) of the thiolated oligonucleotide **4** were next reacted with the gold surfaces by immersing the pretreated gold electrodes for about 16 h at ambient temperature in the deaerated solution protected from light. The Fc-$(dT)_{20}$-modified-gold electrodes were then carefully washed with deionized water and soaked in 1 M aqueous $NaClO_4$ for 30 min in order to remove thoroughly the oligomeric chains noncovalently linked to the gold surface.

Hybridization Procedures. A. Voltammetry at a Bare Gold Electrode. Unthiolated 3′-Fc-$(dT)_{20}$ sequence **2** (∼1 mM) was hybridized in the supporting electrolyte solution by heating to 90 °C for 10 min followed by slow cooling to room temperature. A ca. 100 μL of redox **(2)**-$(dA)_{20}$ duplex solution were then placed in a microwell cell for electrochemical study at a ultramicro- or a millimetric polished gold electrode. **B. Hybridization of a Surface-Bound Fc-$(dT)_{20}$ Monolayer.** Surface hybridization experiments were performed by exposing the gold surface-bound Fc-$(dT)_{20}$ monolayer to 50 μL of a ∼5 μM solution of the full complementary strand $(dA)_{20}$ in 0.1 M $NaClO_4$, 2.5 mM sodium phosphate buffer pH 7.0, for 1 h at 25 °C and then for at least 2 h at 20 °C. The immobilized dsDNA ($(dT\text{-}dA)_{20}$) monolayer electrode was then washed with deionized water and kept in 0.1 M $NaClO_4$ water in a refrigerator until use.

Properties of the Fc-DNA-Modified Gold Electrodes. The Fc-$(dT)_{20}$- (or $(dT\text{-}dA)_{20}$-) modified gold electrodes exhibit excellent electrochemical stability. In particular no decrease in the surface coverage of terminally attached chains was detected after a series of cyclic voltammetry measurements, the investigated potential window extending between −0.1 V and +0.35 V. When not in use, the

(11) Beal, P. A.; Dervan, P. B. *J. Am. Chem. Soc.* **1992**, *114*, 4976−4982.
(12) (a) Anne, A.; Demaille, C.; Moiroux, J. *J. Am. Chem. Soc.* **1999**, *121*, 10379−10388. (b) Anne, A.; Demaille, C.; Moiroux, J. *J. Am. Chem. Soc.* **2001**, *123*, 4817−4825.
(13) Hapiot, P.; Moiroux, J.; Savéant, J.-M. *J. Am. Chem. Soc.* **1990**, *110*, 1337−1343.
(14) Anne, A.; Demaille, C.; Moiroux, J. *Macromolecules* **2002**, *35*, 5578−5586.

electrodes were kept in deaerated aqueous 0.1 M $NaClO_4$ in a refrigerator and could be used for at least 1 month with no appreciable changes in the electrochemical response.

Syntheses. The cystaminyl-protected form **3** of the 5′-thiol 3′-ferrocene-$(dT)_{20}$ oligonucleotide **4** used for immobilization on gold electrodes was synthesized according to the route shown in Scheme 2.

Sulfo-*N*-hydroxysuccinimide of 3-Ferrocenylpropanoic Acid 1. The ferrocene labeling reagent **1** was prepared as follows. To a stirred solution of 3-ferrocenylpropanoic acid (50 mg, 0.19 mmol)[15] in 750 μL of dimethylformamide were added *N*-hydroxysulfosuccinimide (46 mg, 0.21 mmol) and dicyclohexylcarbodiimide (44 mg, 0.21 mmol). The reaction mixture was then allowed to react for 24 h. The insoluble 1,3-dicyclohexylurea was removed by filtration, and cold ethyl/dichloromethane was added to the filtrate. The resulting precipitate was dried in vacuo to yield the activated ferrocene ester Fc-NHS which was used as such in the conjugation step.

3′-Ferrocenylated Oligonucleotide 2, p-5′-$(dT)_{20}$-3′-Fc. A 20 mM solution of ferrocene sulfo NHS ester **1** in aqueous phosphate buffer (pH 8) containing 50% DMSO was prepared and quickly filtered from residual urea through a Millipore 0.45 μm HV membrane before immediate use. In a typical experiment, approximately 20 OD_{260} units of the 5′-amino-modified oligonucleotide, p-5′-$(dT)_{20}$-3′-NH_2 (~0.1 μmol), were dissolved in 215 μL of phosphate buffer (pH 8.0). Then, 85 μL of the ferrocene sulfo NHS ester **1** solution (3.4 μmol) were added. The mixture was allowed to react under stirring for 3 h. At this point, analytical HPLC on Nucleosil C_{18} showed the quantitative conversion of the starting oligonucleotide (t_r = 4.6 min) into the more hydrophobic ferrocene-linked oligonucleotide p-5′-$(dT)_{20}$-3′-Fc (t_r = 13.5 min). The resulting mixture was directly purified by reversed-phase HPLC. Appropriate fractions were dried by lyophilization, and excess salt was removed by repeated lyophilization (×3) with deionized water to yield the triethylammonium salt of **2**. Average yield 95%. MS (MALDI-TOF) (+) data: *m*/*z* $(M + H)^+$, 6556.1, $C_{219}H_{290}N_{41}O_{147}P_{21}Fe$ requires 6555.2. The remarkably similar thermal stability of (**2**)−$(dA)_{20}$ duplex, T_m, 36 °C and unlabeled DNA oligonucleotide, (p-5′-$(dT)_{20}$-3′-NH_2)−$(dA)_{20}$ duplex, T_m, 36 °C, indicates that the presence of the tethered-(C7)-alkylferrocene unit at the 3′-phosphate does not alter the hybridization properties of the oligonucleotide.

5′-Cystaminyl-3′-Ferrocenylated-Oligonucleotide 3, SS−C2−5′-$(dT)_{20}$-3′-Fc. Coupling of cystamine to the 5′-phosphate of Fc-oligonucleotide **2** was performed in DMSO following a general synthetic methodology originally reported by Godovikova et al.[16] and summarized in Scheme 2. Approximately 10 OD_{260} units of the triethylammonium salt of 5′-phosphorylated oligonucleotide **2** were dissolved in 25 μL of dry DMSO. Then 50 μL of a solution containing 4-(*N*,*N*-dimethylamino)pyridine (DMAP) (5 mg, 40 μmol), 2,2′-dipyridyl disulfide (6.6 mg, 30 μmol), and triphenylphosphine (7.9 mg, 30 μmol) in DMSO were added under stirring. After 15 min of activation, cystamine-dihydrochloride was added (5 mg, 22 μmol), and the reaction was allowed to pursue at room temperature for 2 h. The crude 5′-cystamine-oligonucleotide **3** was precipitated from the mixture with 1.5 mL of 3% $LiClO_4$ in acetone, centrifugated, and washed several times with acetone. As judged by analytical RP-HPLC (peak integral) on Supelco Supelcosil 120-5 ABZ^+ Plus (using a linear gradient of acetonitrile in aqueous KH_2PO_4 (20 mM) and $NBu_4KH_2PO_4$ (5 mM), pH 7.5, data not shown), the coupling efficiency was over 80%. RP-HPLC purification was carried out as above for **2** and afforded thiol-protected oligonucleotide **3** in 30% isolated yield (based on starting **2**), with a minimum final purity of about 80%. The identity and purity of the product **3** (when compared to starting material **2**) were confirmed by mass spectrometry analyses. MS (MALDI-TOF) (+) data: *m*/*z* $(M + H)^+$, 6689.9, $C_{223}H_{300}N_{43}O_{146}P_{21}S_2Fe$ requires 6689.4.

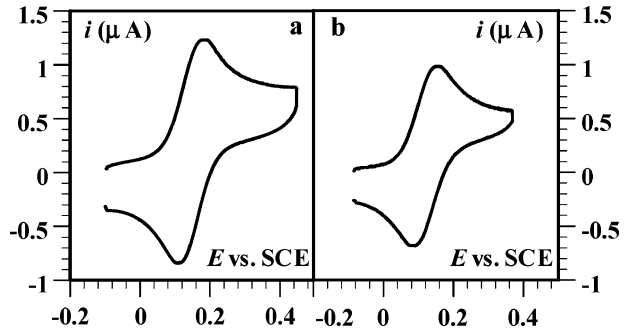

Figure 1. Cyclic voltammograms of a 1mM solution of 20-mer Fc-DNA: (a) Fc-$(dT)_{20}$ (ssDNA), **2**. (b) **2**-$(dA)_{20}$ (dsDNA). The electrode is a 0.5 mm diameter gold disk. Scan rate v = 0.1 V/s. Temperature T = 21 °C. Supporting electrolyte: 1 M $NaClO_4$ + 25 mM sodium phosphate buffer pH 7.

Results

The synthesized redox active ferrocene (Fc)-labeled DNA oligonucleotides Fc-$(dT)_{20}$ (**2**−**4**) used for solution and surface electrochemical studies are shown in Scheme 2. A ferrocene propanoyl moiety was attached through an amino linker to the 3′-end of a commercially available 5′-phosphate $(dT)_{20}$ sequence, using our synthesized sulfo-*N*-hydroxysuccinimide activated ester **1** as the ferrocene labeling reagent. For preparation of the Fc-dT_{20} conjugate **3** containing the cystaminyl residue at the 5′-phosphate (disulfide protected form of **4**), we adopted a simple and reliable coupling procedure[16] based on the combined use of Mukaiyama reagents and nucleophilic catalysis. All Fc-dT_{20} derivatives were characterized by matrix-assisted laser desorption ionization time-of-flight mass spectrometry (MALDI-TOF MS) and exhibited a single sharp *m*/*z* (M + H, positive ion mode) species peak (see Experimental Section).

Cyclic Voltammetry at a Bare Gold Electrode of Fc-ssDNA and Perfect Duplex Fc-dsDNA Freely Diffusing in Solution. For scan rates v < 1 V/s, the cyclic voltammetry behavior at a millimetric gold electrode of ~1 mM ferrocenoyl single- (ss) and double-stranded (ds) DNA, Fc-$(dT)_{20}$ (**2** or **3**), and Fc-$(dT\text{-}dA)_{20}$ duplex in solution was the one expected for planar diffusion of a freely diffusing reversible (Nernstian) redox couple,[17] as shown in Figure 1. In particular, the anodic (E_{pa}) versus cathodic (E_{pc}) peak-to-peak separation ($E_{pa} - E_{pc} = \Delta E_p$) was of ~60 mV and the anodic peak current i_{pa} was proportional to $\sqrt{v}$. The standard potential $E°$ of the DNA-borne-ferrocene head is thus given by the half sum of the anodic and cathodic peak potentials, and $i_{pa} = 0.446FSC°\sqrt{D_tFv/RT}$, where $C°$ is the Fc-DNA strand bulk concentration, S is the electrode surface area, and D_t is the translational diffusion coefficient of the DNA species.[17] The standard potential then measured for the Fc-$(dT)_{20}$ chain is 145 mV/SCE and 120 mV/SCE for the Fc-$(dT\text{-}dA)_{20}$ duplex in good agreement with the $E°$ value of 149 mV/SCE determined earlier for ferrocenepropanoylated-poly(ethylene glycol) Fc-PEG chains.[14] The small negative shift in the redox potential (~ −25 mV) caused by hybridization suggests only slight modifications in the local electronic environment of the

(15) Anne, A.; Blanc, B.; Moiroux, J. *Bioconjugate Chem.* **2001**, *12*, 396−405.
(16) Godovikova, T. S.; Zarytova, V. F.; Maltseva, T. V.; Khalimskaya, L. M. *Bioorg. Khim.* **1989**, *15*, 1246−1252. (b) Boutorine, A. S; Le Douan, T.; Battioni, J. P.; Mansuy, D.; Dupré, D.; Hélène, C. *Bioconjugate Chem.* **1990**, *1*, 350−356.
(17) Andrieux, C. P.; Savéant, J.-M. Electrochemical reactions. In *Investigations of Rates and Mechanisms of Reactions, Techniques in Chemistry*; Bernasconi, C., Ed.; Wiley: New York, 1986; Vol. 6, 4/E, Part 2, pp 305−390.

tethered-ferrocene moiety.[18] When compared to the $E°$ value for the neutral Fc-PEG chains, the redox potentials measured for Fc-DNA indicate that extra anionic charges of the phosphodiester backbone of ss- and dsDNA are comparably well-screened in the chosen 1 M $NaClO_4$ aqueous electrolyte.

Since experiments were run in small volumes, concentration effects unavoidably occurred, preventing the precise knowledge of bulk concentration $C°$ and consequently that of D_t from the sole measurement of i_{pa}. To circumvent these uncertainties in D_t determination, we adopted an experimental approach based on the comparison of the classical peak current i_{pa} with the diffusion-limited plateau current $i_{plateau}$ recorded by steady-state voltammetry at a microelectrode (radius a), given by $i_{plateau} = 4FD_tC°a$.[19] Under such circumstances, the value of D_t can be safely derived from the measured $i_{plateau}/i_{peak}$ ratio, using the following $C°$-independent formula: $D_t = (i_{plateau}/i_{peak} \times 0.1115S/a)^2Fv/RT$.[20] In this work, plateau-shaped cyclic voltammograms were easily obtained for both Fc-DNA at a gold microelectrode ($a = 12.5\ \mu$m), this situation being met for scan rates of about 0.05 V/s and less. Following the above-described procedure, we found $D_t = (2.2 \pm 0.4) \times 10^{-6}$ cm^2/s and $(1.7 \pm 0.4) \times 10^{-6}$ cm^2/s for ss- and dsDNA-Fc, respectively. The small difference between these two values shows that the translational diffusion coefficient of ssDNA is only weakly affected by hybridization. Moreover the D_t values we determined are in reasonable agreement with the values of about 1.5×10^{-6} cm^2/s and 1.1×10^{-6} cm^2/s reported for the diffusion coefficients of ss- and ds-20mer DNA, as measured by several different methods.[21−23]

For $v > 1$ V/s, and up to the highest scan rates explored, the peak current remained proportional to $\sqrt{v}$. This result indicates that Fc-$(dT)_{20}$ adsorption did not occur to any measurable degree and falls in line with literature work demonstrating that homopolymer-dT strands are only moderately prone to adsorption on gold surfaces.[24] Similarly, no adsorption was detected for the Fc-$(dT\text{-}dA)_{20}$ duplex.

However, at high enough scan rates, the peak-to-peak separation increased significantly with scan rate for both ss- and dsDNA. This behavior indicates that the rate of the electron transfer between the Fc redox head and the electrode then contributes to the kinetic control of the faradaic current. The peak-to-peak separation dependence on log(v) then allows us to determine k_s, the heterogeneous rate constant of electron transfer.[25] k_s values of 0.05 ± 0.02 cm/s and 0.10 ± 0.02 cm/s are, respectively, found for Fc-ssDNA and Fc-dsDNA. Both values are significantly lower than the value of $k_s \sim 0.2-0.4$ cm/s measured for freely diffusing dimethanolferrocene.[26] A similar lowering of k_s has also been observed for Fc-labeled poly(ethylene glycol) chains.[14] This trend can probably be ascribed to a depleted ferrocene head concentration at the electrode surface, akin to the monomer depletion phenomenon predicted when polymer chains in solution are in the vicinity of nonadsorbing surfaces.[27]

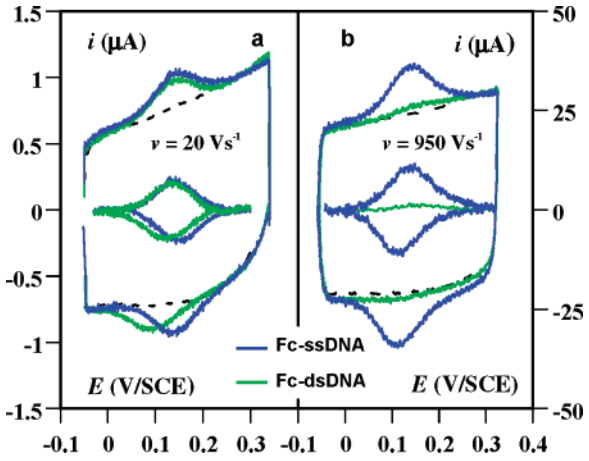

Figure 2. Cyclic voltammograms at a 0.5 mm diameter gold disk electrode bearing a 5′-end-grafted layer of Fc-$(dT)_{20}$, before hybridization (blue trace) and after hybridization by complementary unlabeled dA_{20} strands (green trace). The scan rates are (a) $v = 20$ V/s and (b) $v = 950$ V/s. The dashed curves correspond to background signals recorded after the DNA had been cathodically stripped. Raw and background subtracted signals are shown. Temperature $T = 21$ °C. Supporting electrolyte: 1 M $NaClO_4$ + 25 mM sodium phosphate buffer pH 7.

Quantitative Characterization of the Fc-ssDNA Modified Gold Electrode Employed for Hybridization. The 5′-thiol terminated Fc-$(dT)_{20}$ oligonucleotide **4** (deprotected form of **3**) was reacted with freshly cleaned bare gold electrode surfaces under conditions ensuring saturation coverage in bound $(dT)_{20}$ strands (see Experimental Section). The resulting Fc-$(dT)_{20}$ monolayer system (Scheme 1) having a robust 5′-(*N*)-phosphate-C2-alkylthiolate-gold linkage exhibited a remarkable stability both upon storage and upon repeated voltammetric scans.

Figure 2 illustrates the cyclic voltammetry behavior typically observed for the Fc-ssDNA-modified gold electrode in a 1 M $NaClO_4$ solution, over a scan rate range spanning 4 orders of magnitude, corresponding to an observation time, $\tau_{cv} = RT/Fv$, ranging from 0.1 s to 10 μs.

For low scan rates $v = 0.1$ V/s and up to $v = 500$ V/s, the voltammograms displayed a remarkable symmetrical morphology (Figure 2a). The anodic and cathodic peak currents were proportional to the scan rate while the peak-to-peak potential separation was small, $\Delta E_p \sim 3$ mV at 10 V/s. Such characteristics are typical of the voltammetric signal due to a surface-confined species exhibiting an ideal Nerstian behavior.[28] This result ascertains that all the Fc heads are allowed to reach the electrode surface within the time frame of the voltammogram. Hence,

(18) Pike, A. R.; Ryder, L. C.; Horrocks, B. R.; Clegg, W.; Connolly, B. A.; Houlton, A. *Chem.—Eur. J.* **2005**, *11*, 344−353.
(19) (a) *Microelectrodes: Theory and Applications*; Montenegro, M. I.; Queirós, M. A.; Daschbach, J. L., Eds.; Nato ASI Series E, Kluwer: Boston, 1991; Vol. 197. (b) Amatore, C. In *Physical Electrochemistry. Principles, Methods and Applications*; Rubinstein, I., Ed.; Marcel Dekker: New York, 1995; pp 131−208. (c) Saito, Y. *Rev. Polarogr.* **1968**, *15*, 177.
(20) Amatore, C.; Azzabi, M.; Calas, P.; Jutand, A.; Lefrou, C.; Rollin, Y. *J. Electroanal. Chem.* **1990**, *288*, 45−63.
(21) Stellwagen, E.; Lu, Y.; Stellwagen, N. C. *Biochemsitry* **2003**, *42*, 11745−11750.
(22) (a) Stellwagen, E.; Lu, Y.; Stellwagen, N. C. *Electrophoresis* **2002**, *23*, 2794−2803. (b) Li, S. K.; Ghanem, A.-H.; Teng, C.-L.; Hardee, G. E.; Higuchi, W. I. *J. Pharm. Sci.* **2001**, *90*, 915−931.
(23) (a) Ortega, A.; García de la Torre, J. *J. Chem. Phys.* **2003**, *119*, 9914−9919. (b) Stellwagen, E.; Stellwagen, N. C. *Electrophoresis* **2002**, *23*, 2794−2803. (c) Stellwagen, N. C.; Magnusdóttir, S.; Gelfi, C.; Righetti, P. G. *Biopolymers* **2001**, *58*, 390−397. (d) Lui, H; Skibinska, L.; Gapinski, J.; Patkowski, A.; Fischer, E. W.; Pecora, R. *J. Chem. Phys.* **1998**, *109*, 7556−7566. (e) Eimer, W.; Pecora, R. *J. Chem. Phys.* **1991**, *94*, 2324−2329.
(24) (a) Kimura-Suda, H.; Petrovykh, D. Y.; Tarlov, M. J.; Whitman, L. J. *J. Am. Chem. Soc.* **2003**, *125*, 9014−9015. (b) Demers, L. M.; Östblom, M.; Zhang, H.; Jang, N.-H.; Liedberg, B.; Mirkin, C. A. *J. Am. Chem. Soc.* **2002**, *124*, 11248−11249.
(25) Nicholson, R. S. *Anal. Chem.* **1965**, *37*, 1351−1355.
(26) Abbou, J.; Demaille, C.; Druet, M.; Moiroux, J. *Anal. Chem.* **2002**, *74*, 6355−6363.
(27) de Gennes, P. G. *Scaling Concepts in Polymer Physics*; Cornell University Press: Ithaca, NY, 1991; pp 88−91.

$N_{0,ss}$, the total amount of DNA-bound Fc heads, can be derived from the area under either the anodic or cathodic peak, corrected for background current, yielding for the saturating value $N_{0,ss} = (1.2 \pm 0.1) \times 10^{-14}$ mol. Since one Fc pertains to one chain, the corresponding surface concentration Γ_{ss} in grafted $(dT)_{20}$ chains per cm^2 of effective surface area S_{eff} (measured as described in the Experimental Section) ensues from $\Gamma_{ss} = N_{0,ss}/S_{eff} = (1.6 \pm 0.15) \times 10^{-12}$ mol/cm^2. The value we obtained for Γ_{ss}, in many independent runs, corresponds to less than 5% of a theoretically fully packed monolayer of ~20-mer chains,[29] which means that the system is loosely packed as previously reported. Notably, this low probe density lies in the same range as that of many recent applications that exploit DNA hybridization.[30] The average distance between the anchoring points of the DNA strands is of $\sim 1/\sqrt{\mathcal{N}\Gamma_{ss}} \approx 10$ nm ($\mathcal{N}$ is the Avogadro number) and is thus larger than the contour length of dT_{20} ($\sim L_{ss} = 8.6$ nm). Consequently, it can be safely concluded that there is no lateral interactions between neighboring grafted strands for the present system. The standard potential of the Fc head is determined from the common value of the anodic and cathodic peak potentials of the reversible surface signals yielding $E° = 145$ mV/SCE. This value is identical to the one determined above for the standard potential of Fc-ssDNA freely diffusing in solution, showing that the environment experienced by the Fc heads borne by the strands is similar in both cases. In addition, the peak of the voltammetric signal has a full width at mid-maximum of 95 mV, which is close to the 90 mV predicted for identical, noninteracting tethered redox groups, located outside the charge double layer.[31] At very high scan rates ($\upsilon \geq 1000$ V/s), and as can be seen in Figure 2b, the voltammograms retained the symmetrical morphology typical of surface signals.

As seen in Figure 3a (open symbols), the ratio of the anodic peak current of the voltammograms over the scan rate, i_{pa}/υ, remained constant throughout the explored scan rate range. This behavior indicates either that Fc-$(dT)_{20}$ lies flat on the electrode surface, as a result of the adsorption of its bases, or that the dynamics of the ferrocene head borne by the ssDNA strand is too fast to be characterized, even at the highest scan rate we could access. The possibility of the end-grafted Fc-ssDNA strand lying flat on the electrode can be ruled out, as cyclic voltammetry of Fc-$(dT)_{20}$ in solution indicated that spontaneous adsorption of Fc-DNA did not occur, a result we recently confirmed by electrochemical SECM/AFM measurements (unpublished data). It can thus be concluded that the Fc-ssDNA layer actually consists of isolated coiled DNA chains in a so-called mushroom configuration.[32] The chain size is characterized by the Flory radius R_F which, under high salt conditions and in a good solvent like water, is given by[32] $R_F = l_{pss}(L_{ss}/l_{pss})^{3/5} \approx 4-6$ nm, taking a value of $l_{pss} \approx 1-3$ nm[33] for the persistence length of poly(dT). The Fc-ssDNA layer then behaves in a way

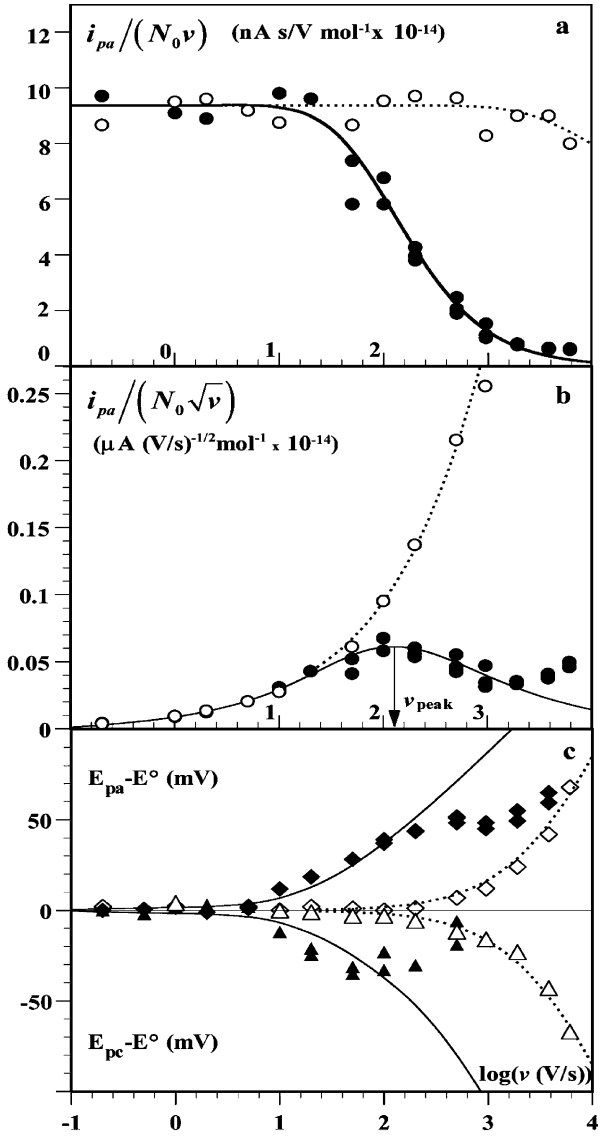

Figure 3. Scan rate υ dependence of the anodic peak current i_{pa} and of the anodic and cathodic peak potentials E_{pa} and E_{pc} of the cyclic voltammograms recorded at a gold electrode bearing a 5′-end-grafted layer of Fc-$(dT)_{20}$, before (open symbols) and after (filled symbols) hybridization by fully complementary $(dA)_{20}$ target. In (a) and (b) the peak current is normalized versus υ and $\sqrt{\upsilon}$, respectively, and versus the total amount of Fc heads ($N_0 = S_{eff} \times \Gamma = 1.2 \times 10^{-14}$ mol before hydridization and 1.05×10^{-14} mol after hybridization). The continuous lines correspond to a theoretical fit of the data obtained for the hybridized DNA layer, using the in-plane elastic bending model with $D_r^e = 2.5\ 10^6\ s^{-1}$, $\theta_{tilt} = 40°$, $\lambda = 30$. The dotted line corresponds to a fit of the data obtained for the nonhybridized DNA layer, using Laviron's theory for surface-bound species[28] with a transfer coefficient of $\alpha = 0.5$ and $k_0 = 4 \times 10^4\ s^{-1}$. The arrow shows how the value of υ_{peak} ~150 V/s is estimated from the experimental data.

equivalent to a thin redox layer,[28b,34] of a thickness comparable in size with R_F,[12a,14] within which diffusion of the Fc head is fast on the time scale of the experiment due to the high flexibility of the ssDNA chain.

The peak-to-peak separation, observed at the highest scan rate explored (Figure 3c, open symbols), indicates that the

(28) (a) Laviron, E. Voltammetric Methods for the Study of Adsorbed Species. In *Electroanalytical Chemistry*; Bard, A. J., Ed.; Marcel Dekker: New York, 1982; Vol. 12, pp 53−157. (b) Laviron, E. *J. Electroanal. Chem.* **1979**, *101*, 19−28.
(29) Steel, A. B.; Levicky, R. L.; Herne, T. M.; Tarlov, M. J. *Biophys. J.* **2000**, *79*, 975−981.
(30) (a) Peterson, A. W.; Wolf, L. K.; Georgiadis, R. M. *J. Am. Chem. Soc.* **2002**, *142*, 14601−14607. (b) Steel, A. B.; Herne, T. M.; Tarlov, M. J. *Anal. Chem.* **1998**, *70*, 4670−4677. (c) Demers, I. M.; Mirkin, R. C.; Reynolds, R. A.; Letsinger, R. L.; Highanian, R.; Viswanadham, G. *Anal. Chem.* **2000**, *72*, 5535−5541.
(31) Smith, C. P.; White, H. S. *Anal. Chem.* **1992**, *64*, 2398−2405.
(32) de Gennes, P. G. *Macromolecules* **1980**, *13*, 1069−1075.
(33) (a) Kuznetsov, S. V.; Shen, Y.; Benight, A. S.; Ansari, A. *Biophys. J.* **2001**, *81*, 2864−2875. (b) Mills, J. B.; Vacano, E.; Hagerman, P. J. *J. Mol. Biol.* **1999**, *285*, 245−257. (c) Tinland, B.; Pluen, A.; Strun, J.; Weill, G. *Macromolecules* **1997**, *30*, 5763−5765.
(34) Hubbard, A. T.; Anson, F. C. In *Electroanalytical Chemistry*; Bard, A. J., Ed.; Marcel Dekker: New York, 1982; Vol. 4, pp 129−214.

electron transfer between the Fc heads and the electrode starts to contribute to the kinetic control of the faradaic current. The variation of both E_{pa} and E_{pc} with $\log(\upsilon)$ can thus be fitted using the theoretical expression of the voltammogram, derived by Laviron[28] in the case of a slow electron transfer to surface-confined species (Figure 3c, open symbols). The only adjustable parameter is then the electron-transfer rate constant k_0, the best fit value of which is found to be of $k_0 = (4 \pm 1) \times 10^4\ s^{-1}$. In the framework of the thin layer model, k_0 is related to k_s and l, the thin layer thickness, by $k_0 = k_s/l$.[28b] Using the value of k_s determined above for Fc-ssDNA strands in solution yields a value of $l = 14 \pm 8$ nm, which is, as expected, comparable with R_F.

Voltammetric Features of the Hybridized Fc-dsDNA Layer. The fully hybridized Fc-dsDNA layer was formed by exposing the Fc-$(dT)_{20}$-modified electrode to a $\sim 5\ \mu$M solution of fully complementary $(dA)_{20}$ target in 0.1 M $NaClO_4$ (pH 7) at 20 °C for at least 2 h and was analyzed by cyclic voltammetry in the regime of very high ionic strength (1 M $NaClO_4$).

At a low enough scan rate, $\upsilon \leq 20$ V/s, the signal recorded for the hybridized DNA monolayer is quite similar to the ideal Nerstian surface voltammogram obtained before hybridization, as evidenced in Figure 2a. The peak current is proportional to the scan rate, while the peak separation is less than 10 mV. The signal is centered around a potential of 120 mV/SCE, which corresponds nicely to the standard potential measured for freely diffusing Fc-$(dT\text{-}dA)_{20}$. Integration of the forward or backward, background subtracted wave leads to a total amount of grafted Fc heads $N_{0,ds} = (1.05 \pm 0.1) \times 10^{-14}$ mol which, assuming a complete hybridization of the layer, would correspond to a dsDNA surface concentration of $\Gamma_{ds} = (1.4 \pm 0.15) \times 10^{-12}$ mol/cm^2. This value of Γ_{ds} is quite lower than the maximum packing density of $\sim 5 \times 10^{-11}$ mol/cm^2 predicted for dsDNA and is comparable to reported results for ~20−25mer dsDNA grafted on gold.[35,36] Even though much more compact dsDNA layers are described in the literature,[7,8,37] the value of Γ_{ds} we obtained is advantageously lower than the highest coverage of $\sim 10^{-11}$ mol/cm^2 allowing complete hybridization of the strands.[38] The comparison of Γ_{ds} and Γ_{ss} indicates that the hybridization process occurs with only a slight (~15%) loss in the anchored Fc-DNA chains.

For $\upsilon > 20$ V/s and as the scan rate was raised, the voltammetric behavior of the Fc-$(dT\text{-}dA)_{20}$-modified electrode was observed to depart from the ideal surface regime recorded for Fc-$(dT)_{20}$. As seen in Figure 3a, the i_{pa}/υ ratio decreased dramatically with increasing scan rate, to such an extent that at high enough scan rate the faradaic signal was hardly distinguishable from the background current (see Figure 2b, $\upsilon = 950$ V s^{-1}). Such an extinction of the dsDNA signal with increasing scan rate can be conveniently represented by plotting the peak current function, defined as the $i_{pa}/\sqrt{\upsilon}$ ratio, versus $\log(\upsilon)$, as shown in Figure 3b. It is seen that whereas the peak current function recorded for ssDNA continuously increases with υ, following the variation predicted for a surface process,[28] the variation corresponding to the $(dT\text{-}dA)_{20}$ duplex is bell-shaped: it departs from the surface-regime curve at $\upsilon \sim 100$ V/s, passes by a maximum at $\upsilon \sim 200$ V/s, before decreasing continuously until $\upsilon \sim 5000$ V/s. At this scan rate the peak current function is only worth $^1/_{10}$ of its value before hybridization. The variations of both E_{pa} and E_{pc} with $\log(\upsilon)$ are presented in Figure 3c (filled symbols). One can see that, for $\upsilon > 10$ V/s, the anodic peak shifts positively, while the cathodic peak potential E_{pc} shifts negatively. The peak potentials then remain approximately constant from $\upsilon > 200$ V/s and up to $\upsilon = 1000$ V/s.

The above voltammetric behavior of the hybridized layer is not compatible with a diffusionless electron transfer from the electrode to the Fc head of dsDNA, which would have resulted in a scan rate independent i_{pa}/υ ratio.[28,39] In contrast, the very fact that the $i_{pa}/\sqrt{\upsilon}$ vs $\log(\upsilon)$ plot deviates from the one corresponding to the surface regime implies that the faradaic current is controlled by the Fc head motional dynamics. However, the Fc head transport mechanism cannot be planar diffusion, or rotational diffusion of the dsDNA around its anchoring point, since for both of these geometries a plateau-shaped $i_{pa}/\sqrt{\upsilon}$ vs $\log(\upsilon)$ plot is expected.[17,40] The occurrence of a maximum in the $i_{pa}/\sqrt{\upsilon}$ vs $\log(\upsilon)$ variation is on the other hand highly reminiscent of the voltammetric behavior of a redox species undergoing *elastic diffusion*, i.e., whose diffusion toward the electrode is hampered by a springlike tether.[12] In the present case diffusional motion of the Fc head necessarily implies bending of the duplex DNA which does act as such a flexible tether. A model describing the voltammetric response of a redox species undergoing elastic bending motion is thus needed to exploit our experimental results and access the dynamics of the duplex DNA quantitatively. Such a model, taking into account the intrinsic elasticity of duplex DNA and the particular geometry of the bending motion, is developed below.

Theory

Bending Conformation and Energy of Short Duplex DNA End-Grafted to a Surface. Like any linear macromolecule, *long* dsDNA chains can be modeled as consisting of a large series of randomly oriented segments. The elasticity of such chains is said to be of entropic nature since it results from the random orientation of the segments. This type of elasticity is typically quantified using the Wormlike Chain model that relates the apparent spring constant of the chain to the effective length of the segments, also referred to as the persistence length l_p. A generally admitted value of l_p for dsDNA chains is of ~50 nm.[41]

In contrast, the elasticity of *short* dsDNA, i.e., shorter than l_p, is not of statistical origin but arises from the isotropic elasticity of the DNA double helix and consequently short sections of DNA are typically modeled as elastic thin rods.[42] Such a modeling approach was shown to be valid down to the

(35) Levicky, R.; Herne, T. M.; Tarlov, M. J.; Satija, S. K. *J. Am. Chem. Soc.* **1998**, *120*, 9787−9792.
(36) Immos, C. E.; Lee, S. J.; Grinstaff, M. W. *ChemBioChem* **2004**, *5*, 1100−1103.
(37) (a) Kelley, S. O.; Barton, J. K.; Jackson, N. M.; Hill, M. G.; *Bioconjugate Chem.* **1997**, *8*, 31−37. (b) Drummond, T. G.; Hill, M. G.; Barton, J. K. *J. Am. Chem. Soc.* **2004**, *126*, 15010−15011.
(38) Peterlintz, K. A.; Georgiadis, R. M.; Herne, T. M.; Tarlov, M. J. *J. Am. Chem. Soc.* **1997**, *119*, 3401−3402.
(39) Actually, at a high scan rate, if the electron transfer becomes irreversible this ratio can decrease by 30% at most, i.e., much less than what is observed here for the ds-DNA (ref 28).
(40) (a) Amatore, C.; Bouret, A.; Maisonhaute, E.; Goldsmith, J. I.; Abruña, H. D. *Chem.—Eur. J.* **2001**, *7*, 2206−2226. (b) Amatore, C.; Bouret, A.; Maisonhaute, E.; Goldsmith, J. I.; Abruña, H. D. *Chem. Phys. Chem.* **2001**, *2*, 130−134.
(41) Bloomfield, V. A.; Crothers, D. M.; Tinoco, I. *Nucleic acids: Structures, Properties and Functions*; University Science Books: Sausalito, CA, 2000.
(42) Grossberg, A. Y.; Khokhlov, A. R. *Statistical Physics of Macromolecules*; American Institute of Physics, New York, 1994; pp 3−14.

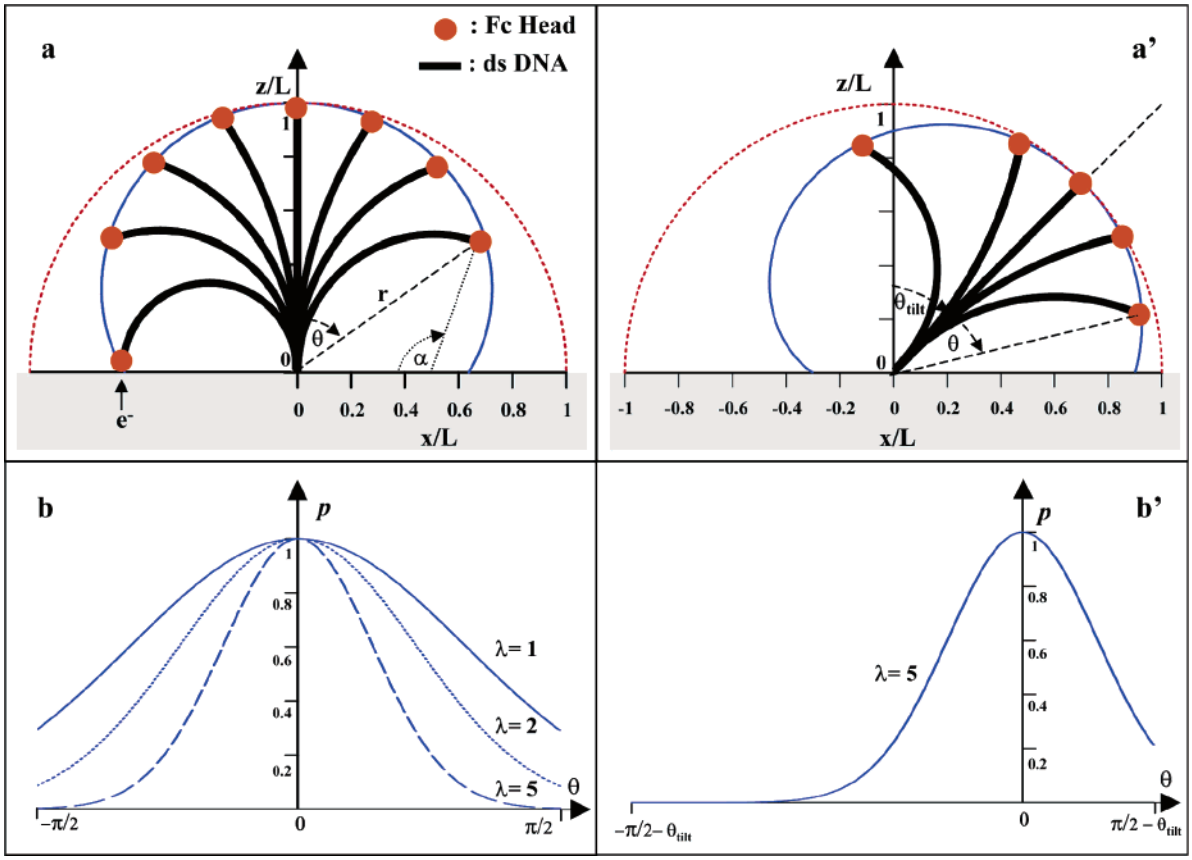

Figure 4. (Top) Schematized bending behavior of Fc-dsDNA end-grafted onto the electrode surface (represented by the gray area). In (a) the DNA strand is grafted perpendicularly to the electrode surface, whereas in (a′) the grafting orientation is tilted by an angle θ_{tilt}. (Bottom) Dimensionless ferrocene head concentration p as a function of the bending angle θ, b and b′ corresponding to the situations depicted, respectively, in a and a′. The value of λ indicated on the curves reflects the DNA-rod rigidity: the stiffer the rod, the higher λ.

level of a few base pairs[43] and is therefore appropriate to describe the elastic property of the 20mer dsDNA used in this work.

We first consider the case of a dsDNA-rod 5′-end grafted in *an upright position* to the electrode surface, as shown in Figure 4a. It is assumed in the following that, as a consequence of the covalent grafting of the DNA chain to the electrode by a *short* C2 linker (∼0.3 nm in length), the attached extremity of the bulky DNA rod (∼2−3 nm in diameter) is located too close to the surface for the rod to have enough room to freely pivot around its grafting point. Therefore the local DNA chain direction at its anchoring point is considered as being constant. We also assume that dsDNA bends with a constant radius of curvature, which is justified by the short contour length of the helix (6.8 nm[41]) with respect to l_p.[42] These simple assumptions allow the bent conformations of the dsDNA-rod to be derived geometrically, a few of them being represented in Figure 4a. The energy E_b required to bend the short dsDNA, assimilated to a cylindrical rod of length L, to a bending angle α, is then given by[41,42]

$$E_b = \frac{1}{2}\kappa\frac{\alpha^2}{L} = 2\frac{\kappa}{L}\theta^2$$

α and θ being defined graphically in Figure 4a and where κ is the bending elasticity modulus of the rod. Incidentally, the elasticity of long dsDNA chains resulting from this local bending behavior, l_p, is related to κ by $l_p = \kappa/k_BT$. From this expression it is clear that low κ values, i.e., short persistence length values, are characteristic of flexible chains.

Motional Dynamics of the DNA Borne Fc Head. During the time course of a cyclic voltammogram, the Fc head travels to and away from the electrode surface as a result of the dsDNA rod bending. Since the hydrophilic C7 tether, linking the Fc head to the 3′-free end of dsDNA, is smaller in size than the contour length of the 20mer dsDNA (∼1 nm at full extinction vs 6.8 nm),[44] the motion of the Fc head is assimilated to the one of the free end of the dsDNA rod. The path of the ferrocene head is thus confined to a 2D shell, the projection of which in any $x-z$ plane containing the rod and perpendicular to the electrode surface is represented as a continuous line in Figure 4a.

The Fc head path in the plane is then given by

$$z = L\frac{\sin 2\theta}{2\theta} \text{ and } x = L\frac{\sin^2\theta}{\theta}$$

where z is the space coordinate perpendicular to the electrode surface and pointing away from it and x is the space coordinate parallel to the electrode surface.

It is noteworthy that the shell along which the Fc heads are free to move differ substantially from a hemispherical shell,

(43) (a) Pakleza, C.; Cognet, J. A. H. *Nucleic Acids Res.* **2003**, *31*, 1075−1085. (b) Santini, G. P. H.; Pakleza, C.; Cognet, J. A. H. *Nucleic Acids Res.* **2003**, *31*, 1086−1096.

(44) Considering its hydrophilicity and length, the tether probably behaves as a short water-soluble oligomer and is actually coiled, i.e., much smaller in size than its fully extended length.

the projection of which is shown as a dotted line in Figure 4a. However the actual shell is still symmetrical around the z axis, and therefore the Fc head motion only has to be calculated for the first quadrant defined, in spherical coordinates (r,θ) as $0 \leq \theta \leq \pi/2$ and

$$r = L\frac{\sin\theta}{\theta} \tag{1}$$

The motion of the ferrocene heads is modeled in the framework of the elastic diffusion model we reported earlier in the case of planar diffusion. This model takes into account the forces acting on each ferrocene head namely a drag force F_{dr}, an osmotic force F_{os}, and a restoring force F_{be}. This latter force arises from the dsDNA rod elasticity that tends to bring back the ferrocene heads toward their equilibrium position, i.e., to the top of the shell. It derives from the bending energy gradient along the shell as

$$F_{be} = -\frac{\partial E_b}{\partial s} = -\frac{\partial E_b}{\partial \theta}\times\frac{\partial \theta}{\partial s} = -k_{be}\theta\frac{\partial \theta}{\partial s}$$

with ∂s the arc element along the shell and $k_{be} = 4\kappa/L$ a bending "elasticity" constant, expressed as a molar quantity, having the dimension of an energy.

In what follows, it should be borne in mind that what is actually modeled here is the collective motion of a vast number of Fc-tagged dsDNA rods behaving identically. As a result the problem of the ferrocene head motion can be treated equivalently by considering either the bending of a single dsDNA strand or the motion of all of the ferrocene heads moving on the surface of a single virtual shell, as if all the noninteracting strands were grafted at the same position on the electrode surface. In the former case the problem would be solved in terms of the probability of finding the ferrocene head on the shell within a given angular range, whether in the latter case the problem can be cast in terms of surface concentration of ferrocene heads on a single *virtual* shell. We find it more convenient to use this latter approach. Furthermore, introducing a fictitious elementary shell thickness ϵ allows us to express the elastic diffusion problem using a ferrocene head volume concentration C.

The sum of the osmotic, dragging, and elastic bending forces is then given by

$$F_{os} + F_{dr} + F_{bd} = -\frac{RT}{C}\frac{\partial C}{\partial s} - k_{dr}\frac{j}{C} - k_{be}\theta\frac{\partial \theta}{\partial s} = 0$$

where k_{dr} is a drag constant which quantifies the friction force experienced by the ferrocene heads.

j is the local flux of ferrocene heads along the shell that is thus given by

$$j = -\frac{RT}{k_{dr}}\left\{\frac{\partial C}{\partial s} + \frac{k_{be}}{RT}\theta\frac{\partial \theta}{\partial s}\right\} = -\frac{RT}{k_{dr}}\frac{\partial \theta}{\partial s}\left\{\frac{\partial C}{\partial \theta} + \frac{k_{be}}{RT}\theta\right\}$$

considering that most of the drag force arises from the friction of the DNA rod on the solvent:

$$\frac{RT}{k_{dr}} \approx D$$

where D is the diffusion coefficient of the DNA rod to be considered here, whose expression is discussed below.

By definition in spherical coordinates, the length of an arc element is given by $\partial s^2 = \partial r^2 + r^2\partial\theta^2$.

From eq 1 it ensues that along the shell

$$\partial\theta/\partial s = \frac{\theta^2}{L\sqrt{\theta^2 + \sin\theta\cos\theta(\tan\theta - 2\theta)}}$$

so that the expression for the elastic bending diffusion flux then is

$$j = -\frac{D}{L}\frac{\theta^2}{\sqrt{\theta^2 + \sin\theta\cos\theta(\tan\theta - 2\theta)}}\left\{\frac{\partial C}{\partial \theta} + \lambda\theta\right\} \tag{2}$$

where λ is a dimensionless elasticity constant of the duplex DNA: $\lambda = k_{be}/RT = 4\kappa/LRT$.

At equilibrium no net current flows through the electrode so that whatever θ, $j = 0$.

From integration of eq 2 it follows that

$$C = C^* \exp[-\lambda\theta^2/2] \text{ with } C^* = C(\theta = 0)$$

Multiplying the above equation by ϵ allows the relation to be expressed in terms of local surface concentration Γ of Fc heads on the shell:

$$\Gamma = \Gamma^* \exp[-\lambda\theta^2/2] \tag{3}$$

the expression of Γ^* is obtained by integration of the surface concentration over the whole shell which must lead to N_0, the total number of ferrocene heads present on the electrode:

$$\Gamma^* = \frac{N_0}{2\pi L^2 G(\lambda)}$$

with

$$G(\lambda) = \int_0^{\pi/2}\frac{\sin^2\theta}{\theta^2}\sqrt{1 + \sin\theta\cos\theta(\tan\theta - 2\theta)/\theta^2}\,\exp[-\lambda\theta^2/2]\,\partial\theta$$

From eq 3 it is seen that the equilibrium concentration profile of the Fc heads on the shell is Gaussian. The larger λ, i.e., the stiffer the dsDNA chain, the more heads gathered on the top of the shell, as shown in Figure 4b.

An equivalent to Fick's second law can be derived by considering the variation dn of the number of ferrocene heads within a stripe of the shell of surface $S = 2\pi\epsilon x = 2\pi\epsilon L\sin^2\theta/\theta$ and of volume Sds, during an elementary time dt:

$$\frac{dn}{dt} = -d(Sj) \text{ so that } \frac{dC}{dt} = -\frac{d(Sj)}{S\,ds}$$

Taking into account the expressions of S and ds as a function of θ given above, one finally arrives to the following time and space dependent differential equation describing the ferrocene head dynamics induced by DNA bending:

$$\frac{\partial C}{\partial t} = \frac{D}{L^2}\left\{A_1(\theta)\frac{\partial C^2}{\partial \theta^2} + A_2(\theta)\frac{\partial C}{\partial \theta} + A_3(\theta)C\right\}$$

with

$$A_1(\theta) = \frac{\theta^4}{\theta^2 + \sin\theta\cos\theta(\tan\theta - 2\theta)}$$

$$A_2(\theta) = \theta^3[2\theta/\tan\theta - 1 + 2(\theta\cos\theta - \sin\theta)^2/(\theta^2 + \sin\theta\cos\theta(\tan\theta - 2\theta)) + \lambda\theta^2]/\theta^2 + \sin\theta\cos\theta(\tan\theta - 2\theta)$$

$$A_3(\theta) = 2\lambda\theta^4[1 + \theta/\tan\theta - (\theta\sin\theta)^2/(\theta^2 + \sin\theta\cos\theta(\tan\theta - 2\theta))]/\theta^2 + \sin\theta\cos\theta(\tan\theta - 2\theta)$$

The D/L^2 term which appears in the above differential equation plays the role of a rotational diffusion coefficient and characterizes the friction of the DNA chain on the solvent during its bending motion. We choose to approximate this term by the rotational diffusion coefficient D_r^e calculated for an end-tethered *rigid* DNA rod rotating around its anchoring point which can be derived using the so-called "shish-kebab" model.[45] It can be shown (see Supporting Information) that the thus obtained end-rotational diffusion coefficient D_r^e is one-fourth of the usually considered rotational diffusion coefficient for rods. This difference arises from the fact that usual rotational diffusion coefficients correspond to the rotation of rods around their center of mass, whereas here the rod rotates around its anchored end.

Theoretical Elastic Bending Diffusion Cyclic Voltammogram. In cyclic voltammetry the electrode potential E is scanned from an initial potential E_i negative enough with respect to the ferrocene/ferrocenium couple for the ferrocene heads to be in their reduced state. Their equilibrium surface concentration profile on the shell Γ_p is therefore given by eq 3.

Upon scanning the potential positively the Fc heads reaching the electrode surface are oxidized as

$$P \overset{E^\circ}{\rightleftharpoons} Q + e^-$$

where P and Q respectively stand for the reduced and oxidized form of the ferrocene head. E° is the standard potential of the redox couple. The dynamics of the dsDNA strand bending does not depend on the redox state of the Fc head it bears, thus the following conservation expression holds for any value of θ and time t:

$$\Gamma_P(\theta) + \Gamma_Q(\theta) = \Gamma^* \exp[-\lambda\theta^2/2]$$

Therefore the elastic bending diffusion problem needs to be solved only for the reduced ferrocene head.

At the electrode surface ($\theta = \pi/2$) assuming that the electron transfer is Nersntian, i.e., fast as compared to the DNA-bending dynamics:

$$\Gamma_P(\pi/2) = \Gamma_Q(\pi/2)\exp[-F(E - E^\circ)/RT]$$

At the electrode surface, the concentration of the reduced form of the ferrocene head on the shell is then related to the electrode potential by

$$\Gamma_P(\pi/2) = \Gamma^* \exp[-\lambda\pi^2/8]/(1 + \exp[F(E - E^\circ)/RT])$$

A dimensionless formulation of the elastic bending diffusion problem can then be obtained using the following change of variable:

$$\tau = D_r^e t,\ p = \Gamma_p/\Gamma^*,\ \xi = F(E - E^\circ)/RT$$

The linear variation of the electrode potential with time is then given by $\xi = \beta\tau - \xi_i$, where ξ_i is the dimensionless initial potential, taken negative enough for the voltammogram not to depend on its exact value,[17] and $\beta = Fv/RTD_r^e$. This later parameter compares the characteristic rotational diffusion time $1/D_r^e$ to the cyclic voltammetry observation time RT/Fv.

The dimensionless current ψ to be calculated is related to the actual current i by $\psi = i/(FN_0D_r^e)$.

It is also convenient to introduce the following current function: $\psi^* = \psi/\sqrt{\beta}$, which is the dimensionless equivalent of the $i/\sqrt{v}$ ratio used above to present the experimental data.

The partial differential equation to be solved is then

$$\frac{\partial p}{\partial \tau} = A_1(\theta)\frac{\partial p^2}{\partial \theta^2} + A_2(\theta)\frac{\partial p}{\partial \theta} + A_3(\theta)p \qquad (4)$$

together with the following initial and boundary conditions:

$$\tau = 0,\ \forall\ \theta:\ p = \exp[-\lambda\theta^2/2]$$

$$\tau > 0,\ \theta = \pi/2:\ p(\pi/2) = \exp[-\lambda\pi^2/8]/(1 + e^{\xi})$$

and for reasons of symmetry at $\theta = 0$: $j = 0$ and thus, from eq 2, $(\partial p/\partial\theta)_0 = 0$.

The voltammetric current is derived from the local flux expressed at $\theta = \pi/2$ (eq 2), summed up along a circular strip of radius $2L/\pi$ and of width ϵ representing the footprint of the shell on the electrode surface to yield

$$i = F \times 2\pi \times (2L/\pi)\epsilon \times j(\pi/2) = -FD\frac{\pi^2}{\sqrt{\pi^2/4 + 1}}\left\{\left(\frac{\partial\Gamma_p}{\partial\theta}\right)_{\pi/2} + \lambda\frac{\pi}{2}\Gamma_p(\pi/2)\right\}$$

the corresponding dimensionless expression being

$$\psi = -\frac{1}{G(\lambda)\sqrt{1 + 4/\pi^2}}\left\{\left(\frac{\partial p}{\partial\theta}\right)_{\pi/2} + \lambda p_{\pi/2}\pi/2\right\}$$

The dimensionless voltammogram depends solely on the β and λ parameters and, in the general case, is calculated by solving numerically the partial differential eq 4 as described in the Supporting Information. The simulations allowed the limiting situations presented below to be identified.

$\beta \to 0$, $\forall\ \lambda$: Surface Regime. The potential scan rate is slow enough, as compared to the DNA bending dynamics, so that ample time is given to all of the Fc heads to reach the electrode surface and exchange an electron with it. Therefore, no information regarding the bending dynamics can be obtained from the signal.

The dimensionless current is then given by

$$\psi = \beta\frac{\exp[-\xi]}{(1 + \exp[-\xi])^2}$$

while the corresponding anodic current is

(45) Doi, M.; Edwards, S. F. *The Theory of Polymer Dynamics*; Oxford University Press: Oxford, 1986; pp 291−295.

$$i = \frac{F^2 N_0 \upsilon}{RT} \frac{\exp[-F(E - E^\circ)/RT]}{(1 + \exp[-F(E - E^\circ)/RT])^2}$$

This expression is identical to the one predicted for the Nernstian behavior of a redox species irreversibly adsorbed to an electrode.[28] The anodic and cathodic peak potentials are equal to E°, and the peak current is proportional to the scan rate.

Integration of this surface signal leads to N_0, the total amount of Fc heads (and thus of dsDNA) present at the electrode surface.

$\beta \rightarrow +\infty$, $\forall\ \lambda$: **Planar Diffusion Regime.** This case corresponds to the scan rate being so large that only the ferrocene heads present near the electrode surface at equilibrium are detected during the time course of the cyclic voltammogram. The Fc head motion takes place over such a short distance that, despite the elastic behavior and the particular geometry of the diffusion field, it is still equivalent to simple planar diffusion. Such a behavior has already been described in the case of both planar elastic bounded diffusion[12] and simple diffusion along spherical shells.[40] The morphology of the voltammogram calculated for this limiting situation is indeed similar to the one expected for planar diffusion.[17] However, the equivalent redox species concentration to consider is the one at the electrode surface $C(\pi/2)$ so that the peak current is

$$i_p = 0.446 F S_e C(\pi/2) \sqrt{FD\upsilon/RT}$$

with S_e the effective electrode surface area, i.e., the shell foot print area, $S_e = 4L\epsilon$.

It ensues that $i_p = 0.446F4L\Gamma(\pi/2)\sqrt{FD\upsilon/RT}$ and, finally, replacing $\Gamma(\pi/2)$ by its value given by eq 3:

$$i_p = 0.284 F N_0 \sqrt{D_r^e F\upsilon/RT} \frac{\exp[-\lambda\pi^2/8]}{G(\lambda)}$$

the corresponding dimensionless anodic peak current thus being

$$\psi_p = 0.284 \sqrt{\beta} \frac{\exp[-\lambda\pi^2/8]}{G(\lambda)} \qquad (5)$$

In the general case, the introduction of an elastic contribution to the dynamics of the redox heads induces large changes of the voltammetric behavior as compared to simple diffusion. In particular the variation of the intensity and of the morphology of the cyclic voltammograms with scan rate is deeply affected by the presence of an elastic force.

This is illustrated by the cyclic voltammograms presented in Figure 5, calculated for a high value of $\lambda = 10$ and increasing values of β, a situation that mimics an increase of scan rate in the case of a quite stiff rod. As β is increased from low values corresponding to the surface wave situation described above (Figure 5a), the peak separation initially increases and the wave broadens so that the signal takes an aspect resembling the one of a diffusional wave (Figure 5b). As β is further increased the signal morphology continues to change until a plateau-shaped signal is obtained (Figure 5c). This situation, only observed for high enough values of lambda ($\lambda > \sim 5$), corresponds to the case where the DNA-rod supporting the Fc head is so rigid that most of the heads remain gathered at the top of the shell. The Fc heads reach the electrode surface in a low stationary flux.

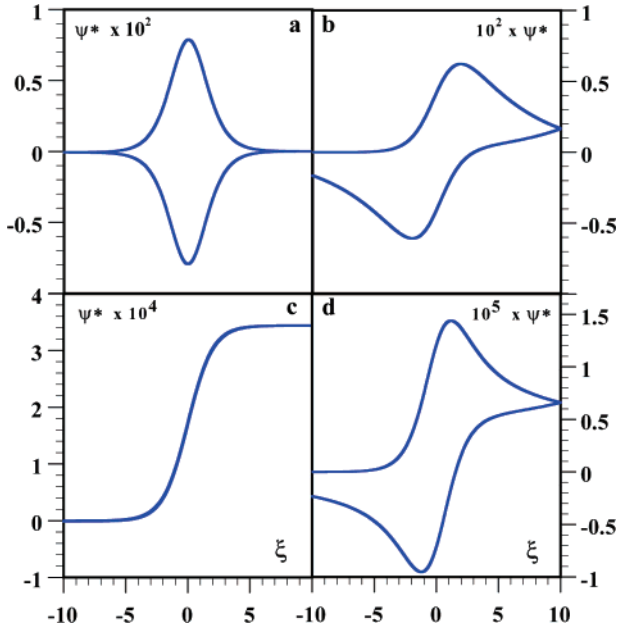

Figure 5. Elastic bending diffusion cyclic voltammograms calculated using the shell model in the case of stiff rods ($\lambda = 10$) and for increasing values of β: (a) $\beta = 1 \times 10^{-5}$, (b) $\beta = 3.16 \times 10^{-3}$, (c) $\beta = 3.16$, (d) $\beta = 1 \times 10^5$.

In such a case the sigmoid-shaped wave is described by the equation:

$$\psi = \frac{2}{\pi G(\lambda) K(\lambda)} \frac{1}{1 + e^{-\xi}} \text{ with } K(\lambda) = \int_0^{\pi/2} \frac{\sqrt{\theta^2 + \sin\theta\cos\theta(\tan\theta - 2\theta)}}{\theta^2} \exp[\lambda\theta^2/2]\, \partial\theta$$

or

$$i = 0.637 \frac{F N_0 D_r^e}{G(\lambda)\, K(\lambda)} \frac{1}{1 + \exp[-F(E - E^\circ)/RT]}$$

Interestingly in this *stationary regime* the voltammogram is scan rate independent.

As β (i.e., υ) is increased further, the situation corresponding to the limiting case described above for $\beta \rightarrow +\infty$ is reached and the voltammogram becomes anew peak-shaped (Figure 5d), its height being proportional to $\sqrt{\upsilon}$.

The variation with β of the dimensionless anodic peak current function ψ_{pa}^* and peak potentials of the voltammograms, calculated for a large range of λ values, are reported, respectively, in Figure 6a and 6b.

Whatever the value of λ, at low enough β values, the peak current function increases smoothly with β. As explained above, the voltammogram then corresponds to a surface signal[28] for which $\psi_p = 0.25\beta$ so that $\psi_p^* = 0.25\sqrt{\beta}$. In other words, at slow enough scan rate the peak height is proportional to υ, no matter λ. However, the stiffer the rod (the higher λ), the lower the scan rate at which this behavior is observed.

Upon increasing β the peak current function levels off and passes through a maximum before decreasing asymptotically toward a constant value reached for high enough β values. This behavior corresponds to the attainment of the planar diffusion

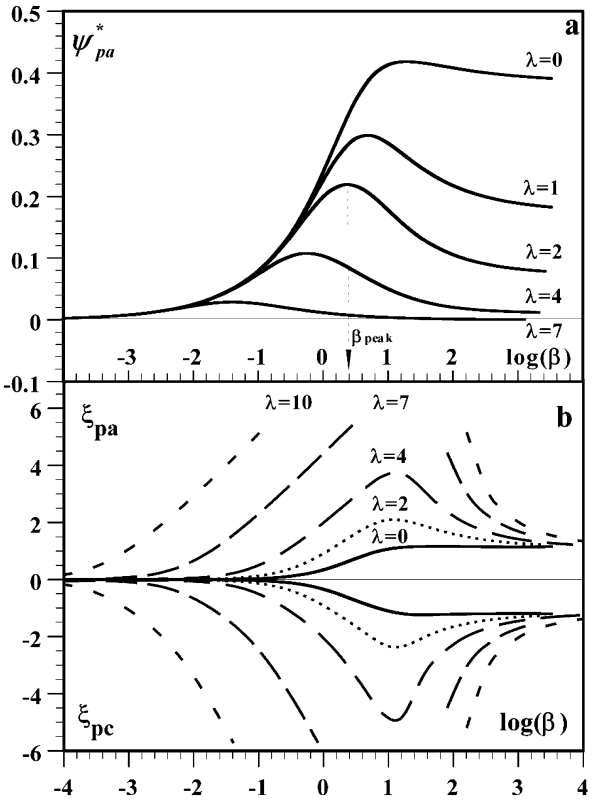

Figure 6. Variation as a function of log(β) of (a) the dimensionless peak current function (ψ^*_{pa}) and of (b) the dimensionless anodic (ξ_{pa}) and cathodic (ξ_{pc}) peak potentials of the elastic bending diffusion voltammograms, calculated using the shell model, for the values of λ indicated on each curve.

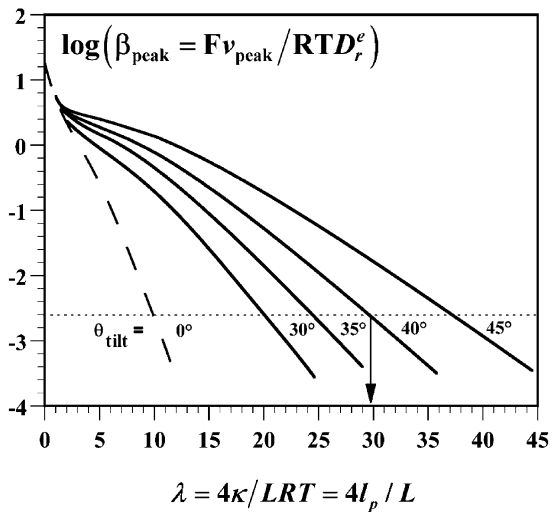

Figure 7. Working curves allowing the elasticity modulus κ, i.e., the persistence length l_p, of grafted dsDNA rods to be determined from cyclic voltammetry data (proceeding as described in the text). λ dependence of the peak value β_{peak} of the ψ^*_{pa} vs β variation (see Figure 6) for various dsDNA tilt angle values θ_{tilt}. The dashed line curve gives the calculated variation using the shell model for $\theta_{tilt} = 0$. Each continuous curve gives the calculated variation for a given θ_{tilt} value using the in-plane elastic bending diffusion model. λ is defined as $\lambda = 4\kappa/LRT = 4l_p/L$, with L as the contour length of the dsDNA rod. β_{peak} is given by $\beta_{peak} = Fv_{peak}/(RTD^e_r)$, with v_{peak} as the scan rate for which the $i_{pa}/\sqrt{v}$ vs log(v) variation is observed to pass by a maximum and D^e_r as the end-rotational diffusion coefficient of the dsDNA rod. The horizontal dotted line corresponds to a β_{peak} value of 2.3×10^{-3} calculated using a value of $D^e_r = 2.5 \times 10^6$ s^{-1} and the experimental value of $v_{peak} = 150$ V/s. The arrow shows how the corresponding value of $\lambda \sim 30$, characterizing the bending elasticity of the grafted (dT-dA)$_{20}$ duplex, is read from the curve calculated for $\theta_{tilt} = 40°$.

regime, and the peak current function value is then a rapidly decreasing function of λ given by eq 5.

Interestingly, the peak current function vs β variation is peak-shaped *even for* $\lambda = 0$; this specific behavior is related to the diffusion along *nonhemispherical* shells.[40] However the peak is much more pronounced for $\lambda > 0$, and for $\lambda > 2$, the ψ^*_p vs log(β) variation develops a bell-like shape characteristic of elastic diffusion.[12]

The effect of elastic bending diffusion on the calculated variation of the peak potentials with β also bears strong resemblance with the one reported in the case of planar elastic bounded diffusion.[12] At low enough β values the forward and backward peak potentials are equal to $E°$, as expected for a surface wave. As β is increased both peaks shift away in opposite directions. For $\lambda > \sim 5$ this shift is linear with a slope of ~60 mV per unit of log β (at 25 °C); the higher λ, the lower the β values for which this linear shift is observed. Finally when the limiting situation corresponding to $\beta \rightarrow +\infty$ is reached, $\xi_{pa} = -\xi_{pr} = 1.1$ so that the peak separation is 60 mV at 25 °C.[17]

Practical Characterization of Elastic Bending Diffusion by Cyclic Voltammetry. The log(β_{peak}) vs λ Working Curve. The existence of a maximum in the ψ^*_{pa} vs β (i.e., $i_p/\sqrt{v}$ vs log(v)) variation is the most striking feature of the cyclic voltammetric characterization of elastic bending diffusion. As seen in Figure 6a, the location of this maximum along the β axis, denoted β_{peak}, solely depends on the value of λ. Taking advantage of this, the plot presented in Figure 7, showing the dependence of β_{peak} on λ, can be used as a working curve to determine the bending elasticity modulus κ of the experimental system under investigation, proceeding as follows. The scan rate v_{peak} at which the maximum of the $i_p/\sqrt{v}$ vs log(v) variation is experimentally observed can be converted into a β_{peak} value, provided that the value of D^e_r is known, since $\beta_{peak} = RT/(Fv_{peak}D^e_r)$ and the value of λ (that is ultimately of κ, since $\lambda = 4\kappa/LRT$) can then be directly read from the abscissa of the working curve. It can also be seen from the working curve that the value of β_{peak} (i.e., of v_{peak}) is predicted to depend sharply on the value of λ (i.e., of κ), especially at high λ: varying λ by 20% results in a variation of β_{peak} of about 1 order of magnitude (for $\lambda = 10$). This shows that cyclic voltammetry is potentially an extremely sensitive method to determine the bending elasticity of end-grafted duplex DNA.

Dependence of the Voltammetric Behavior on the dsDNA Tilt Angle. "In-Plane Elastic Bending Model". It has been reported that thiolated dsDNA anchored by their 5′-end were not standing onto the electrode surface in an upright position, as assumed so far, but were tilted by as much as 45° toward it.[46] It is intuitively expected that such a tilt would affect the cyclic voltammetry response of Fc-dsDNA since the equilibrium position of the ferrocene heads would then be located closer to the electrode surface. The above elastic bending diffusion model was therefore improved to introduce a rod tilt angle parameter,

(46) (a) Kelley, S. O.; Barton, J. K.; Jackson, N. M.; McPherson, L. D.; Potter, A. B.; Spain, E. M.; Allen, M. J.; Hill, M. G. *Langmuir* **1998**, *24*, 6781−6784. (b) Zhou, D.; Sinniah, K.; Abell, C.; Rayment, T. *Langmuir* **2002**, *18*, 8278−8281. (c) Dong, L. Q.; Zhou, J. Z.; Wu, L. L.; Dong, P.; Lin, Z. H. *Chem. Phys. Lett.* **2002**, *354*, 458−465. (d) Zhang, Z.-L.; Pang, D.-W.; Zhang, R.-Y.; Yan, J.-W.; Mao, B.-W.; Qi, Y.-P. *Bioconjugate Chem.* **2002**, *13*, 104−109. (e) Ceres, D. M.; Barton, J. K. *J. Am. Chem. Soc.* **2003**, *125*, 14964−14965.

as shown in Figure 4a′. The equilibrium position of the ferrocene head is tilted toward the electrode by an angle θ_{tilt}, and the ferrocene head position is still referred to the angle θ measured from the equilibrium position. Consequently, the equilibrium distribution of the ferrocene heads is still a Gaussian centered around $\theta = 0$ (as shown in Figure 4b′), but the Fc head path is modified since the whole shell is tilted. In particular the diffusion path toward the electrode is no longer symmetrical around $\theta = 0$: the electrode surface is closer to the $\theta = 0$ point following the path in the tilt direction than it is following the opposite direction. This loss of symmetry requires the problem to be formulated and solved in a two-dimensional spherical coordinate system. However, the problem can be kept unidimensional if the diffusion of the ferrocene heads is restricted to within the $x-z$ plane containing the tilted dsDNA. The diffusion path is no longer a shell but a ringlike path as represented in Figure 4a′. Such an in-plane elastic bending diffusion model is expected to provide a better description of the actual dynamical motion of the Fc head the more important the tilt angle and the stiffer the dsDNA rod.

The Fc heads can then be brought in contact with the electrode surface by the dsDNA bending toward it either in the direction of the tilt or in the opposite direction. So that θ is allowed to vary from $\theta_{min} = -\pi/2 - \theta_{tilt}$ to $\theta_{max} = \pi/2 - \theta_{tilt}$.

The formal expression of the second Fick's law is still given by eq 4. But the θ dependent coefficients $A_2(\theta)$ and $A_3(\theta)$ are modified as follows:

$$A_2(\theta) = \frac{\theta^3[2(\theta\cos\theta - \sin\theta)^2/(\theta^2 + \sin\theta\cos\theta(\tan\theta - 2\theta)) + \lambda\theta^2]}{\theta^2 + \sin\theta\cos\theta(\tan\theta - 2\theta)}$$

$$A_3(\theta) = \frac{\lambda\theta^4[3 - 2(\theta\sin\theta)^2/(\theta^2 + \sin\theta\cos\theta(\tan\theta - 2\theta))]}{\theta^2 + \sin\theta\cos\theta(\tan\theta - 2\theta)}$$

the initial and boundary conditions being now

$$\tau = 0, \forall\ \theta:\ p = \exp[-\lambda\theta^2/2]$$

$$\tau > 0, \theta = \pi/2 - \theta_{tilt}:\ p(\pi/2 - \theta_{tilt}) = \exp[-\lambda(\pi/2 - \theta_{tilt})^2/2]/(1 + \exp[\xi])$$

$$\tau > 0, \theta = -\pi/2 - \theta_{tilt}:\ p(-\pi/2 - \theta_{tilt}) = \exp[-\lambda(-\pi/2 - \theta_{tilt})^2/2]/(1 + \exp[\xi])$$

The current is calculated by summing the flux of Fc heads arriving at the electrode at $\theta = \pi/2 - \theta_{tilt}$ and at $\theta = \pi/2 - \theta_{tilt}$ so that the expression of the dimensionless current is

$$\psi = \frac{1}{G'(\lambda,\theta_{tilt})}\left[T(\theta_{min})\left\{\left(\frac{\partial p}{\partial\theta}\right)_{\theta_{min}} + \lambda p_{\theta_{min}}\theta_{min}\right\} - T(\theta_{max})\left\{\left(\frac{\partial p}{\partial\theta}\right)_{\theta_{max}} + \lambda p_{\theta_{max}}\theta_{max}\right\}\right]$$

with

$$G'(\lambda,\theta_{tilt}) = \int_{-\pi/2-\theta_{tilt}}^{\pi/2-\theta_{tilt}} \frac{\sqrt{\theta^2 + \sin\theta\cos\theta(\tan\theta - 2\theta)}}{\theta^2}\exp[-\lambda\theta^2/2]\,\partial\theta$$

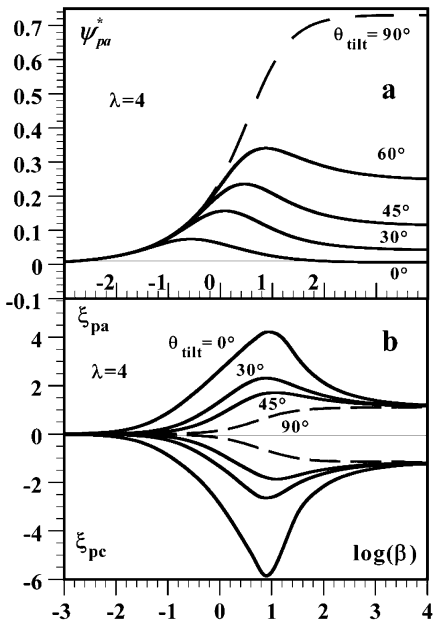

Figure 8. Effect of tilting the dsDNA grafting orientation on the characteristics of the elastic bending diffusion cyclic voltammograms. Variation with log(β) of (a) the dimensionless peak current function ψ^*_{pa} and of (b) the dimensionless anodic and cathodic peak potentials of the voltammograms ξ_{pa} and ξ_{pc} calculated using the in-plane elastic bending diffusion model with $\lambda = 4$ and for values of θ_{tilt} indicated on each curve.

and

$$T(\theta) = \frac{\theta^2}{\sqrt{\theta^2 + \sin\theta\cos\theta(\tan\theta - 2\theta)}}$$

Numerical resolution of the partial differential equation (eq 4) yields the theoretical voltammogram for any set of θ_{tilt}, λ, and β values (see Supporting Information for details).

To check the validity of this in-plane elastic bending diffusion model, the simulated voltammetric behavior for $\theta_{tilt} = 0$ was compared to the one calculated with the shell model described above. It was found that even in this worst case scenario both models yielded similar results for $\lambda \geq 4$. Thus the in-plane elastic bending diffusion model is expected to be a fortiori correct for $\theta_{tilt} > 0$ and $\lambda \geq 4$.

The limiting voltammetric regimes, and corresponding morphologies of the faradaic signal, described above for the shell model, are also predicted by the in-plane elastic bending model for any value of $\theta_{tilt} < 90°$. However the analytical expressions for the corresponding voltammograms are slightly different and are given in Supporting Information.

The tilt angle dependence of the voltammetric behavior of an end-grafted Fc-dsDNA rod is exemplified in Figure 8 where the characteristics of cyclic voltammograms calculated for $\lambda = 4$, and for increasing values of θ_{tilt}, are plotted as a function of β.

It is seen that as θ_{tilt} is increased from 0° to 90 °, the variation of the peak current function and peak potentials with scan rate gradually lose the signature of elastic diffusion. In particular the bell-shaped variation of the peak current function vs scan rate progressively disappears. An extreme case corresponds to the rod lying flat on the electrode surface ($\theta_{tilt} = 90°$) for which, no matter the rod flexibility, and even though a Gaussian equilibrium distribution of the ferrocene head toward the solution

is also predicted, the features indicative of elastic diffusion are lost (see Figure 8, dashed line).

The system then behaves in a way expected for the planar diffusion of a redox species in a thin-layer cell configuration.[34] Nevertheless, for reasonable values of θ_{tilt} ($<60°$) the voltammetric behavior typical of elastic diffusion is maintained, an increase in θ_{tilt} simply having the same effect as a decrease in λ (compare Figure 6 and Figure 8). This effect is quantified in Figure 7 where the values of β_{peak}, calculated for various values of θ_{tilt}, are plotted as a function of λ. One can see that, for a given value of β_{peak} (i.e., for a corresponding experimental υ_{peak} value), the λ value to be read from the working curve strongly depends on the value of θ_{tilt}: the higher the tilt, the higher the corresponding stiffness λ. Therefore, quantifying λ, i.e., the persistence length of duplex DNA, from the analysis of voltammetry data, requires that the value of θ_{tilt} is known independently. Equivalently, this also means that the orientation of a duplex DNA of known persistence length can be deduced from cyclic voltammetry data. In either case, the necessary log(β_{peak}) vs λ working curve can be calculated for any value of θ_{tilt}, using the analytical expression (eq S1) given in the Supporting Information. Finally it is worth emphasizing that the strong dependence of β_{peak} on the value of λ is largely maintained even when the rod is tilted by as much as $\theta_{tilt} = 45°$: a 30% variation of the DNA-rod stiffness would then translate into an order of magnitude shift in υ_{peak}.

Discussion

Probing the Dynamics of Fc-dsDNA Monolayers by Cyclic Voltammetry. A. Determination of the Persistence Length of Fc-(dT-dA)$_{20}$ Using the In-Plane Elastic Bending Model. The peculiar characteristics of the voltammetric behavior of the hybridized Fc-DNA monolayer that we reported previously and reproduced again here[4] are very well accounted for by the model of elastic bending diffusion developed in the present work. In particular the bell-shaped variation of the peak current function with scan rate not only is theoretically predicted but also can be exploited, in the framework of this model, to derive the persistence length of dsDNA from the voltammetric data. This can be carried out using the working curve reported in Figure 7, provided that the value of D_r^e, the end-rotational diffusion coefficient of the dsDNA rod, and the duplex orientation, defined by θ_{tilt}, are known. In situ AFM[36,46a,b,d,e] and neutron reflectivity studies[35] of layers of dsDNA oligomers, 5′-anchored onto gold surfaces, have shown that, whatever the packing-density, the duplex adopted a preferred upward orientation with an average angle between the double helix and the surface normal of ~30°−45°. It was further demonstrated that, when grafted onto an electrode, the duplex could reorientate reversibly as a function of the electrode potential for potentials higher than 0.25 V/SCE.[46a,c,d,e] At less positive potentials the duplex orientation was observed to be potential-independent, the strand tilt angle then being ~40° with respect to the surface normal.[46a,c,d,e] Consequently, since the peak potentials of the voltammograms recorded here fall within this latter potential region, we take for the tilt angle of the duplex Fc-DNA a constant value of $\theta_{tilt} = 40°$. The end-rotational coefficient D_r^e of the duplex DNA is given by $D_r^e = D_r/4$ where D_r stands for the rotational diffusion coefficient of the Fc-(dT-dA)$_{20}$ duplex (see Supporting Information). Taking for D_r the literature value of $D_r = 10^7$ s^{-1}, as determined by dynamic light scattering experiments for 20mer dsDNA,[22a] yields $D_r^e = 2.5 \times 10^6$ s^{-1}. Using this value of D_r^e, the experimental value of $\upsilon_{peak} \approx (150 \pm 50)$ V/s (Figure 3b) is then converted into $\beta_{peak} = F\upsilon_{peak}/(RTD_r^e) = (2.4 \pm 0.8) \times 10^{-3}$ and a value of $\lambda \approx 30 \pm 1$ is read from the working curve of Figure 7 calculated for $\theta_{tilt} = 40°$. It is worth emphasizing that the value of λ thus derived is relatively immune to any uncertainty on the value of υ_{peak} or D_r^e, since changing β_{peak} by a factor of, e.g., 2 only modifies the read λ value by less than 10%. The entire experimental bell-shaped variation of the peak current function with scan rate can then be quantitatively reproduced using the in-plane elastic bending diffusion model, with $\theta_{tilt} = 40°$ and $\lambda = 30$, a very good adjustment being observed between the experimental and the calculated variation for $\upsilon \leq 1000$ V/s (Figure 9a).

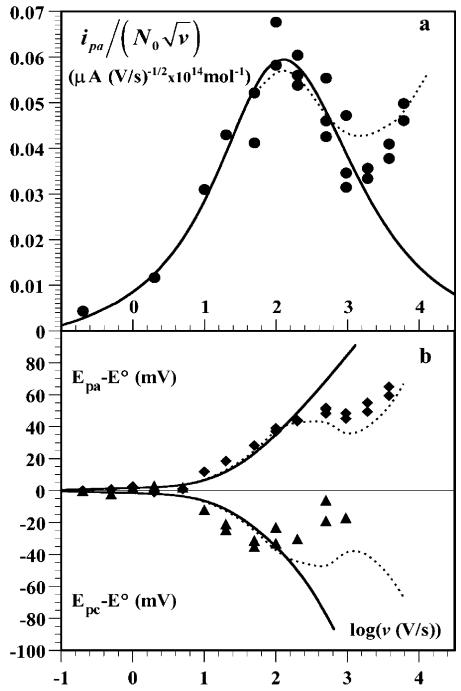

Figure 9. Scan rate υ dependence of the characteristics of the voltammograms recorded at an electrode bearing a layer of Fc-(dT-dA)$_{20}$. (a) Bell-shaped variation of the anodic peak current function $i_{pa}/(N_0\sqrt{\upsilon})$ vs log(υ), with $N_0 = 1.05 \times 10^{-14}$ mol, the total amount of Fc heads present. (b) Variation of the anodic and cathodic peak potentials E_{pa} and E_{pc} vs log(υ). The symbols correspond to the experimental data. The continuous lines correspond to the theoretical values calculated using the in-plane elastic bending model with $D_r^e = 2.5 \times 10^6$ s^{-1}, $\theta_{tilt} = 40°$, $\lambda = 30$. The dotted line is calculated assuming that 5% of the strands remain nonhybridized.

The experimental peak potential variation with scan rate can also be reasonably well fitted by the theoretical variation calculated using the in-plane elastic bending model for $\upsilon < 500$ V/s (see Figure 9b). Moreover the morphology of the experimental signals is found to closely resemble that of the voltammograms simulated for the above values of D_r^e, θ_{tilt}, and λ (Figure 10).

The bending elasticity modulus κ of Fc-(dT-dA)$_{20}$ can then be derived knowing the value of λ since $\kappa = Lk_{be}/4 = \lambda Lk_BT/4$. Taking for L the literature value of 6.8 nm, reported for the length of the (dT-dA)$_{20}$ duplex, leads to $\kappa = (2.07 \pm 0.07) \times 10^{-28}$ J m or, in terms of persistence length, to $l_p = \kappa/k_BT = \lambda L/4 = 51 \pm 2$ nm. This latter value is in very good agreement with the persistence length values reported for poly(dT).poly-

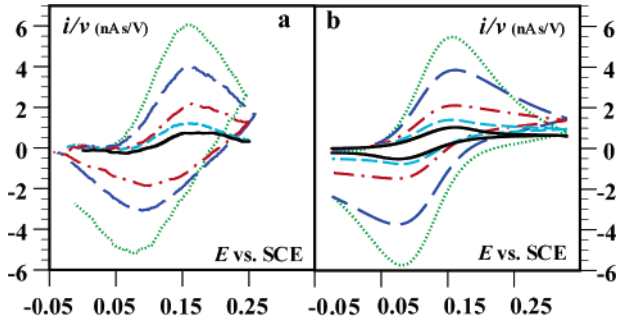

Figure 10. (a) Cyclic voltammograms recorded at an electrode bearing a layer of Fc-(dT-dA)$_{20}$ duplexes. The scan rates are as follows: υ (in V/s) = 100 (···), 200 (− −), 500 (− ·), 950 (- - -), and 1900 (—). The current i, in nA, is normalized versus the scan rate υ, in V/s. (b) The corresponding theoretical voltammograms simulated using the in-plane elastic bending model with $D_r^e = 2.5 \times 10^6$ s^{-1}, $\theta_{tilt} = 40°$, $\lambda = 30$ and allowing for the presence of a fraction of 5% of nonhybridized chains in the layer. In (a) the experimental voltammograms are background subtracted. The cathodic (backward) traces of the voltammograms recorded at 950 V/s and 1900 V/s are not shown. The Fc-dsDNA surface concentration is of $\Gamma = 1.4 \times 10^{-12}$ mol/cm^2. The electrode is a 0.5 mm diameter gold disk. Temperature $T = 21$ °C. Supporting electrolyte: 1 M $NaClO_4$ + 25 mM sodium phosphate buffer pH 7.

(dA) strands, which range from 43 to 51 nm (125−150 bp at 0.34 nm/bp[41]), as measured by triplet anisotropy decay techniques.[47] Such a result strongly substantiates our claim that the intrinsic bending elasticity of DNA controls the dynamics of electron transport in molecular layers of surface grafted redox-tagged dsDNA. It also validates the use of cyclic voltammetry and of the elastic bending diffusion model as a powerful tandem to quantify the elastic behavior of end-grafted short DNA oligomers.

The dependence of the value determined for l_p, on the value taken for θ_{tilt}, is worth discussing as we have theoretically shown that both of these parameters control the voltammetric behavior in a similar way. Allowing θ_{tilt} to vary between the reported duplex tilt angle values of 30° to 45° yields λ values ranging from 20 to 37, i.e., l_p values ranging from 34 to 65 nm. This length interval encloses the range of l_p values reported for poly-(dT)·poly(dA) (43−51 nm), confirming that the duplex tilt angle lies somewhere between 30° and 45°. If it is now l_p which is allowed to vary from 43 to 51 nm (i.e. λ = 25 to 30), a significantly narrower range of possible tilt angles for (dT-dA)$_{20}$ is obtained from Figure 7: $35° \leq \theta_{tilt} \leq 40°$. It is worth emphasizing that, as mentioned above, simple rotational motion of the dsDNA around its anchoring point would have resulted in a voltammetric behavior very different from the one observed here.[40] In particular the salient feature of a bell-shaped peak current function would not have been predicted in this case. Moreover the characteristic time of the system, then simply given by $\tau_r = 1/D_r^e = 0.4\ \mu$s, would have been so fast that scan rates higher than $\upsilon = RT/F\tau_r = 65$ kV/s would have been required to access the chain dynamics. The fact that we could probe the dynamics of the anchored duplex DNA at scan rates 2 orders of magnitude lower than this demonstrates that the motional dynamics of end-tethered DNA oligomers is controlled by bending elasticity rather than by rotational diffusion.

B. Evaluation of the Hybridization Efficiency of End-Grafted Redox ssDNA. For υ >1000 V/s the experimental peak current function is seen to slowly increase with scan rate instead of decreasing as predicted (Figure 9a). This slight departure from the bell-shaped curve can be attributed to the growing contribution to the overall current of the faradaic signal due to the small fraction of redox ssDNA chains that remained nonhybridized. Whereas the current resulting from the elastic bending motion of the hybridized strands levels off with increasing scan rate, the intensity of the surfacelike signal due to the nonhybridized strands continuously increases with υ, ultimately becoming the dominant signal at high scan rates, as evidenced in Figure 3b. The overall voltammetric current i can then be expressed as the weighted average of i_{ds}, the current due to the hybridized chains, and of i_{ss}, the surface signal current due to nonhybridized chains: $i = \gamma\, i_{ss} + (1 - \gamma)\, i_{ds}$, with γ as the fraction of nonhybridized chains. The theoretical peak current function can then be calculated, using for i_{ds} the value predicted by the elastic bending diffusion model, while the value of i_{ss} is calculated using the theoretical expression for the voltammetric response of a thin-layer cell,[28b] and the value of k_0 determined above. A slow increase of the peak current function is then theoretically predicted for υ > 1000 V/s (Figure 9a, dotted line), while the part of the bell-shaped curve recorded for υ < 1000 V/s (the one we exploited so far) remains largely unaffected. The nonhybridized fraction γ of surface-bound Fc-DNA can be quantified by adjustment between the experimental and the theoretically predicted $i_p/\sqrt{\upsilon}$ dependence on scan rate for υ > 1000 V/s, leading to $\gamma \approx 5\%$. The unusual shape of the peak potential vs log(υ) variation, observed for the Fc-dsDNA layer, is then also reproduced by theory (Figure 9b, dotted line). In particular, whereas the elastic bending diffusion of Fc-dsDNA predicts a continuous shift of peak potentials with scan rate, the contribution of the nonhybridized Fc-DNA strands to the overall voltammetric signal results in the peak potentials becoming almost scan rate independent from υ = 200 V/s and up to υ = 1000 V/s. This highly unusual E_p vs log(υ) variation can thus be used as a very sensitive diagnostic criteria for the presence of minute fractions of nonhybridized strands within a layer of dsDNA. For υ > 1000 V/s, the shift of the peak potentials can be largely attributed to the rate of electron transfer between the Fc head of the nonhybridized chains coming into play. This is made obvious in Figure 3c where it is seen that, as the scan rate is raised above 1000 V/s, the E_{pa} and E_{pc} vs log(υ) variations measured for the hybridized layer tend toward the variation measured before hybridization. The high hybridization efficiency of ∼95%, measured for the present system, demonstrates that the molecular recognition capability of the C2-thiolated Fc-(dT)$_{20}$ strands was largely preserved upon their grafting onto a gold surface.

Conclusion

The dramatic changes of the voltammetric behavior of a molecular layer of 5′-end-grafted 3′-ferrocenylated -(dT)$_{20}$ strands, upon hybridization by fully complementary (dA)$_{20}$ target, were demonstrated to reflect the large difference in flexibility between ssDNA and its fully complementary duplex. Before hybridization the Fc-ssDNA layer was shown to behave as a diffusionless system, due to the high flexibility, i.e., the very fast dynamics, of the Fc-(dT)$_{20}$ strand. After hybridization the unique voltammetric behavior of the Fc-(dT-dA)$_{20}$ layer, notably characterized by an unusual bell-shaped variation of

(47) Hogan, M.; LeGrange, J.; Austin, B. *Nature* **1983**, *304*, 752−754.

the peak current function with scan rate, could be fully accounted for making use of the elastic bending diffusion model developed in the present work. This model describes the motion of the DNA-borne ferrocene as resulting from the elastic bending of the duplex DNA toward and away from the electrode. Analysis of the voltammetric data, in light of this unprecedented model, allows the elasticity of the DNA duplex to be quantified. The good agreement between the experimental and theoretical voltammetric behavior we observe, together with the persistence length value of $\sim 51 \pm 2$ nm, typical of poly(dT)·poly(dA) strands, we determined for the duplex DNA, validates the use of our model and demonstrates that dsDNA bending elasticity fully controls the dynamics of electron transport in 5′-anchored redox-labeled dsDNA layers. The ensuing extremely high sensitivity of the cyclic voltammetric response to the flexibility of the end-grafted DNA duplex should allow us to quantify minute alterations of the bending elasticity of dsDNA, associated with base sequence, mismatch, or improper pairing.

Supporting Information Available: Simulation programs to calculate dimensionless cyclic voltammograms of a redox species undergoing elastic bending diffusion are available from the authors upon simple request. Details on the calculation of the end-rotational diffusion coefficient for a terminally anchored thin rod. Expressions of the dimensionless peak current for the in-plane elastic bending model in the limiting situations of surface, planar diffusion, and stationary regime. Analytical expression for the working curve relating β_{peak} to λ for any value of θ_{tilt}. Details on the numerical simulation of the cyclic voltammograms of a species undergoing elastic bending diffusion. This material is available free of charge via the Internet at http://pubs.acs.org.

JA055112A